Research article

JGS
Journal of the Geological Society

https://doi.org/10.1144/jgs2023-108 | Vol. 181 | 2024 | jgs2023-108

Constraining reducing conditions in the Prague Basin during the late Silurian Lau/Kozlowskii extinction event

Lindsi J. Allman[1]*, Chelsie N. Bowman[1], Jiří Frýda[2,3], Nevin P. Kozik[1], Jeremy D. Owens[1] and Seth A. Young[1]

[1] Department of Earth, Ocean & Atmospheric Science, National High Magnetic Field Laboratory, Florida State University, Tallahassee, FL 32306, USA
[2] Faculty of Environmental Sciences, Czech University of Life Sciences Prague, Prague, Czech Republic
[3] Czech Geological Survey, Klárov 3/131, 118 21 Prague 1, Czech Republic

LJA, 0000-0001-8577-6788; CNB, 0000-0001-9052-7014; JF, 0000-0003-2410-3293; NPK, 0000-0001-7759-7552; JDO, 0000-0002-0530-2177; SAY, 0000-0001-6885-4780

* Correspondence: lja15@fsu.edu

Abstract: The Silurian was marked by repeated extinctions, carbon cycle volatility and significant intervals of climatic change. The most notable of these events were the Ludfordian Lau/Kozlowskii extinction and the associated Mid-Ludfordian Lau C isotope excursion, both of which have been linked to a period of global cooling and expanded reducing conditions in the global ocean. We present new data that characterize the marine palaeoredox conditions of the Prague Basin, a peri-Gondwanan terrane. We use I/Ca ratios to assess the local redox conditions in a shallow water carbonate succession and Fe speciation and redox-sensitive trace element concentrations to assess the local redox conditions of a deeper water sequence. Consistently low I/Ca values in the shallow water section suggest either persistent local low-oxygen conditions or possibly diagenetic overprinting. Fe speciation data suggest that the bottom water redox conditions in the deeper shelf setting were consistently anoxic with possible intermittent euxinia. Concentrations of redox-sensitive trace elements consistently higher than upper continental crust values also indicate persistent reducing conditions in the deeper part of the basin. These local redox proxy data from the Prague Basin, including trends in new pyrite S isotope ($\delta^{34}S_{pyr}$) data, are consistent with previous findings of the expansion of anoxic and/or euxinic oceanic conditions. These data, derived from a mid-palaeolatitude marine setting, fill an important gap in our current global dataset for this interval of the late Silurian.

Supplementary material: All the geochemical data reported and discussed herein are available in the Supplemental Data Tables at https://doi.org/10.6084/m9.figshare.c.7008107

Thematic collection: This article is part of the Chemical Evolution of the Mid-Paleozoic Earth System and Biotic Response collection available at: https://www.lyellcollection.org/topic/collections/chemical-evolution-of-the-mid-paleozoic-earth-system

Received 30 June 2023; **revised** 20 November 2023; **accepted** 18 December 2023

During the last three decades, the Silurian has been recognized as an extremely dynamic period in Earth history. An oscillatory climatic transition from the icehouse of the Late Ordovician to the greenhouse conditions of the Devonian (e.g. Jeppsson 1990; Bickert *et al.* 1997; Cramer and Saltzman 2007) was accompanied by repeated marine extinctions and faunal reorganizations (e.g. Jeppsson and Landing 1998; Crampton *et al.* 2016), extreme carbon cycle volatility (e.g. Kaljo *et al.* 1997; Saltzman 2001, 2002; McAdams *et al.* 2019) and notable variations in marine redox conditions (Bowman *et al.* 2019, 2020, 2021; Rose *et al.* 2019; Young *et al.* 2019, 2020; del Rey *et al.* 2020, 2023; Frýda *et al.* 2021*a*, *b*; Zhang *et al.* 2022).

Among these recurring extinction events was the Ludfordian (Ludlow Epoch) Lau/Kozlowskii extinction (LKE), which was the most severe extinction event in the Silurian and at least the tenth most severe in Earth history, with a loss of *c.* 23% of marine genera (Sepkoski 1996; Bond and Grasby 2017). The LKE is named after the 'Lau bioevent' in conodonts from carbonate platform successions (Jeppsson 1990) and the 'Kozlowskii bioevent' in graptolites from deeper water shales (Koren' 1993; Urbanek 1993). The LKE is associated with the Mid-Ludfordian Lau C isotope excursion (Lau CIE, also known as the MLCIE), one of the highest magnitude CIEs in the Phanerozoic, with peak excursion values typically between +5 and +9‰ (Munnecke *et al.* 2003; Calner 2008; Saltzman and Thomas 2012).

The marine extinction slightly predates the onset of the Lau CIE, but both are now hypothesized to be caused by an expansion of reducing conditions in the global oceans (Munnecke *et al.* 2003; Stricanne *et al.* 2006; Bowman *et al.* 2019; Frýda *et al.* 2021*b*). This is evidenced not only by geochemical proxy data, such as S isotopes (Bowman *et al.* 2019), U isotopes (del Rey *et al.* 2020, 2023) and Ba isotopes (Zhang *et al.* 2022), but also by the curiously asynchronous nature of the LKE. Documented extinctions in benthic and nektonic taxa – such as brachiopods (Talent *et al.* 1993; Mergl *et al.* 2018), fish (Eriksson *et al.* 2009), polychaetes (Tonarová *et al.* 2012), cephalopods (Manda 2008), trilobites (Manda and Frýda 2014) and conodonts (e.g. Jeppsson and Aldridge 2000) – precede extinctions in planktic fauna – such as graptolites (Koren' 1993; Urbanek 1993) and acritarchs (Stricanne *et al.* 2006) – suggesting that reducing conditions expanded from deeper to shallower marine waters (Bowman *et al.* 2019; Frýda *et al.* 2021*b*).

Recent analysis of seawater surface temperature changes (Frýda *et al.* 2021*b*) using conodont apatite $\delta^{18}O$ records from different regions located in temperate (Prague Basin and Carnic Alps) as well as tropical (Gotland) palaeolatitudes points to significant global cooling during the Lau CIE. The marked decrease in sea surface temperatures (inferred from the positive shift in $\delta^{18}O_{apatite}$ of at least 3‰) recorded in temperate water areas of the Prague Basin and Carnic Alps (peri-Gondwana), as well as in the tropical areas of Baltica (Laurussia) and

© 2024 The Author(s). Published by The Geological Society of London. All rights reserved. For permissions: http://www.geolsoc.org.uk/permissions. Publishing disclaimer: www.geolsoc.org.uk/pub_ethics

Australia (Gondwana), coupled with a significant eustatic sea-level fall recorded by sequence stratigraphy on all corresponding palaeocontinents, point to glaciation (the Mid-Ludfordian glaciation; see Frýda *et al.* 2021*b*) in polar and subpolar Gondwana.

To date, the majority of marine redox proxy data for the LKE have come from tropical epicontinental basins of the palaeocontinents Baltica and Laurentia (e.g. Bowman *et al.* 2019; 2020, 2021; del Rey *et al.* 2020). Recent studies by Frýda *et al.* (2021*b*), Zhang *et al.* (2022) and del Rey *et al.* (2023) have reported the first marine redox proxy dataset of redox-sensitive trace element concentrations and Ba and U isotopes, respectively, from temperate palaeolatitudes of the Perunica peri-Gondwanan terrane (Kosov Quarry in Czech Republic; Fig. 1b).

Here, we present additional shale-based proxy records from the Kosov Quarry to assess local to regional deep shelf redox conditions in more detail, including pyrite S isotopes ($\delta^{34}S_{pyr}$), Fe speciation and redox-sensitive trace element concentration data. Also presented herein are I/Ca ratios and pyrite S isotope ($\delta^{34}S_{pyr}$) redox proxy data from the shallow shelf carbonate succession of the Mušlovka Quarry Section in the Prague Basin. Key information and references for local redox proxy dynamics are summarized in Figure 2. Using these palaeoredox proxy datasets, we reconstruct how the regional redox conditions of the Prague Basin changed throughout the Ludfordian Stage with respect to both the LKE and Lau CIE. The data and environmental reconstructions discussed here are of particular interest because they offer a detailed perspective on the local expression of these global environmental changes from the mid-palaeolatitude Gondwanan margin.

Geological setting and biostratigraphy

The Mušlovka Quarry and Kosov Quarry (No. JF195) sections are both near modern day Prague in the Czech Republic and were deposited in the Prague Basin of the Barrandian Terrane located between 25 and 30° south of the equator during the Ludfordian (Fig. 1a; Lehnert *et al.* 2007; Frýda and Manda 2013; Tasáryová *et al.* 2014). This basin formed on submerged continental crust inundated by shallow seas and bounded by deeper marine settings. The Barrandian crustal block is debated to have been either an accretion of peri-Gondwanan terranes or the small microcontinent often called Perunica (Havlíček *et al.* 1994; Cocks and Torsvik 2002; Stampfli *et al.* 2002). The Central Bohemian region of the modern Czech Republic provides a variety of outcrops with a diversity of marine lithofacies deposited during the late Silurian, ranging from shallow shelf coarse-grained carbonate facies to deep shelf graptolite shale–mudstone successions. The Ludfordian strata of the Prague Basin make up the upper Kopanina Formation, which is composed of shallow shelf carbonate facies at Mušlovka Quarry (Figs 3a–e, 4) and deeper water interbedded carbonates–marls and shales at Kosov Quarry (Figs 3f, g, 5 and 6).

There was active faulting and volcanism in the Prague Basin during the late Silurian, which led to the development of rapid facies changes over short distances due to variable subsidence and uplift rates (Havlíček and Štorch 1990; Kříž 1991, 1992; Manda and Kříž 2006; Lehnert *et al.* 2007; Frýda and Manda 2013; Tasáryová *et al.* 2018). This early to middle Paleozoic tectonic activity is thought to be associated with continental rifting in the Barrandian Terrane, which never reached an oceanic stage with the production of mid-ocean ridge basalts (e.g. Štorch 1998; Tasáryová *et al.* 2018). In particular, the Kosov Quarry section (Fig. 1b) was located near the Silurian Kosov Volcanic Centre deposited in the latest Wenlock interval. Volcanic activity occurred in this area from the Homerian through Gorstian stages of the mid- to late Silurian (Tasáryová *et al.* 2014). The volcanic rocks are overlain by Ludfordian marine sedimentary strata. These include the interbedded shales–mudstones and carbonates of Kosov Quarry, which are the remnants of an offshore deep shelf setting (Lehnert *et al.* 2007).

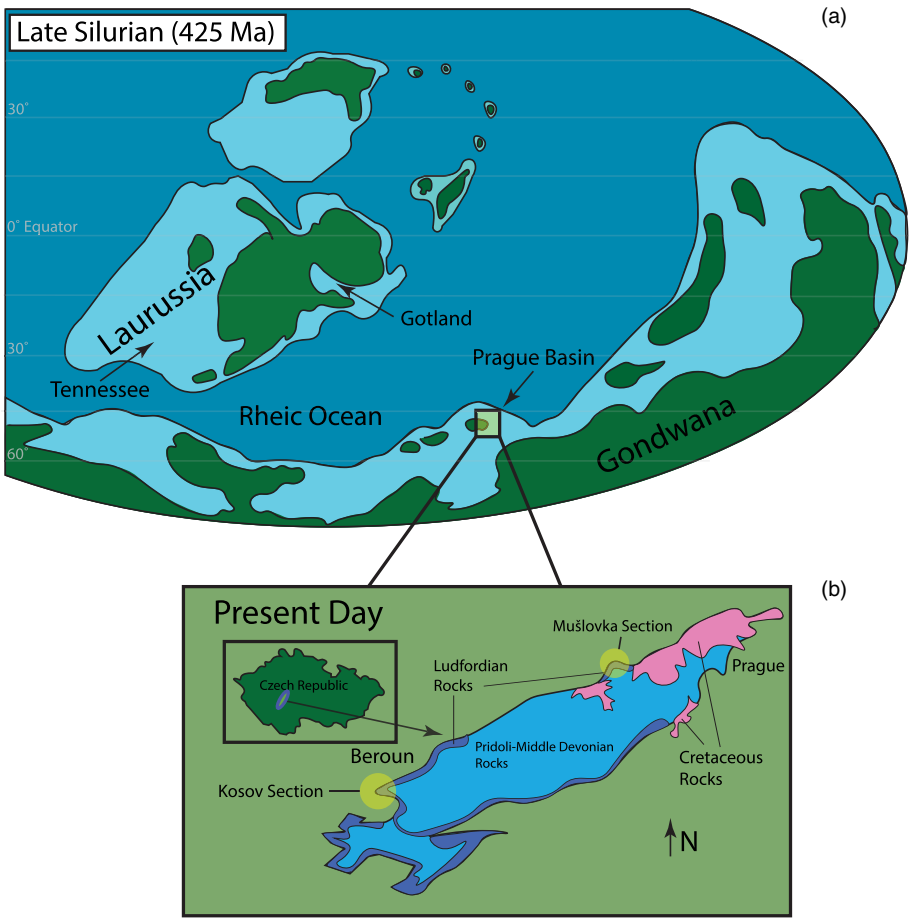

Fig. 1. (**a**) Palaeogeographical reconstruction of the late Silurian (*c.* 425 Ma). (**b**) Distribution of the rocks of the Barrandian Terrane in the Central Bohemian Region of the present day Czech Republic with the Mušlovka and Kosov Quarry sections highlighted by yellow circles. Source: part (a) modified from Scotese (2014); part (b) modified from Frýda *et al.* 2021*a*).

This was followed by the Variscan Orogeny, which formed during the closure of the Rheic Ocean from the Devonian to the Pennsylvanian as part of the assembly of Pangaea (Rölich 2007; Tasáryová *et al.* 2018). The strata of the Prague Basin (Ordovician to Middle Devonian) are thought to have been buried between 1 and 4 km during the Variscan Orogeny (Vacek and Žák 2019). By the Cretaceous, this region was dominated by variable extensional and compressional tectonics related to the motion between the European and African plates, which continued into the Neogene (Hrubcová *et al.* 2010). The collision of these two plates led to the formation of the Alpine–Carpathian Orogeny and the uplift and exposure of the Paleozoic strata of the Barrandian Terrane (Hrubcová *et al.* 2010).

The outcrops in this region serve as a reference for peri-Gondwanan biostratigraphy in the mid-Paleozoic, with detailed work carried out on the Silurian through early Devonian successions (Havlíček and Štorch 1990; Kříž 1991, 1992). Given the presence of both peri-Gondwanan and Baltic–Avalonian–Laurentian fauna, the Prague Basin was well connected to the Rheic Ocean (Kříž 1999, 2008; Manda 2008). The age of deposition for the Mušlovka Quarry section has been well constrained by conodonts (Kříž and Schönlaub 1980; Slavík *et al.* 2014) and by graptolites and conodonts for Kosov Quarry (Štorch 1995; Frýda *et al.* 2021*b*).

The sampled interval of the Kopanina Formation at Mušlovka Quarry encompasses the *Neocucullograptus inexpectatus* graptolite zone in the lowest part of the section, the *Neocucullograptus kozlowskii* zone – the last appearance datum of which defines the Kozlowskii graptolite extinction – and the *Monograptus latilobus* and *Monograptus fragmentalis* graptolite zones in the upper part of the section (Fig. 4; Urbanek 1993; Štorch 1995; Manda *et al.* 2012; Manda and Frýda 2014). Also present within the lower part of the section is the *Polygnathoides siluricus* conodont zone, the practical last appearance datum of which defines the Lau conodont extinction; the *Pedavis latialata–Ozarkodina snajdri* interval zone in the upper part of the section (Fig. 4; Kříž and Schönlaub 1980; Jeppsson 2005).

The Mušlovka Quarry section consists of *c.* 17 m of exposed shallow water carbonates of the Kopanina Formation located outside Prague, Czech Republic (Lehnert *et al.* 2003, 2007; Figs 3a–e, 4). The lowest *c.* 4 m of the sampled interval is a wackestone to packstone with cephalopods, echinoderm fragments, brachiopods, sponges, ostracods and graptolites. The upper 13 m of the section is mudstone to wackestone with fewer and less diverse macrofossils, such as echinoderm fragments, brachiopods, cephalopods and sponges. There are three intervals of flat-pebble conglomerate facies in the upper part of the section (e.g. 4.5–5.0 m, 6.0–6.5 m and 8.0–13.0 m levels) made up of *c.* 10 cm long, 2–3 cm thick clasts (Fig. 2b–d). The clasts in the upper two flat-pebble conglomerate intervals are often coated grains with sub-concentric laminations (Fig. 2b, c). A heavily dolomitized interval is present in the middle of the measured section from 3.0 to 13.0 m (Fig. 2d, e). The likely once micritic matrix of the flat-pebble conglomerate intervals is completely altered with the growth of subhedral to euhedral dolomite and the wackestone to grainstone flat-pebble conglomerate clasts are partially dolomitized. The uppermost 1.5 m of the section are notably laminated and interbedded lime mudstones and black shale. Finely disseminated pyrite is found throughout the section (e.g. Fig. 2e), with some intervals having secondary pyrite present within common secondary calcite veins and infilling bioclastic intraparticle pore spaces.

In the Kosov Quarry, the base of the section begins in the *N. inexpectatus* graptolite zone, above which is the *N. kozlowskii* graptolite zone (Figs 5, 6). Following this is the *Pristiograptus dubius postfrequens* partial range interval graptolite zone. In the upper part of the section is the combined *M. latilobus–Slovenograptus balticus* zone and then the *M. fragmentalis* zone.

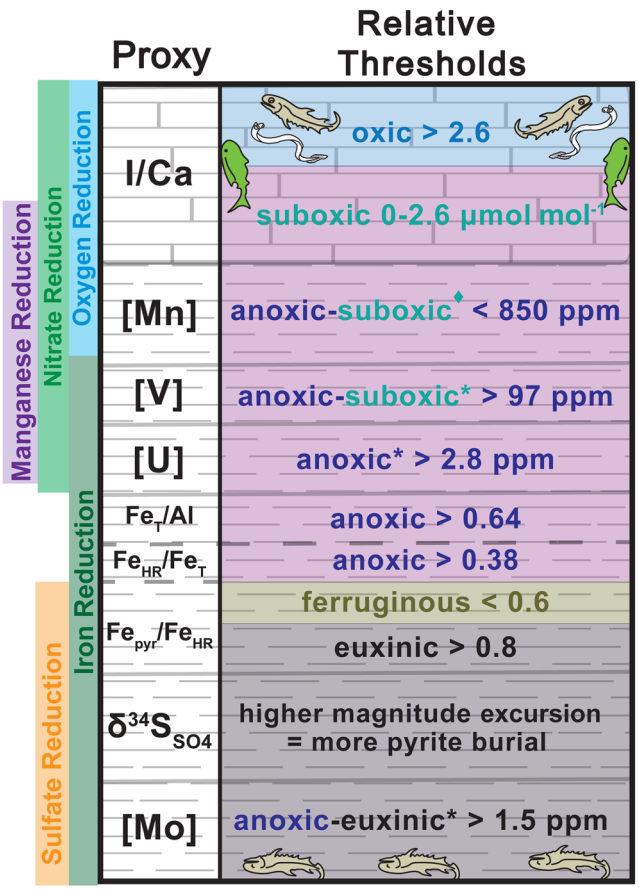

Fig. 2. Schematic diagram of the marine redox proxies used in the present study. Proxies are in order of their relative sensitivity to redox conditions based on the marine redox ladder. The appropriate lithology for each proxy is denoted by the grey background pattern (bricks, carbonate; dashes, shale/mudstone). Threshold values for I/Ca ratios from Z. Lu *et al.* (2016); Mn concentrations from Morford and Emerson (1999), V concentrations from Rudnick and Gao (2003); U and Mo concentrations from McLennan (2001); Fe speciation (Fe_T/Al, Fe_{HR}/F_T, Fe_{pyr}/Fe_{HR}) from Raiswell *et al.* (2008), Raiswell and Canfield (1998) and März *et al.* (2008). Threshold value for Mn represents average oxic marine sediments and the values for V, U and Mo are upper continental crust values. The asterisks (*) indicate threshold values corresponding to upper continental crust values, concentrations above which likely indicate reducing conditions; the diamond shapes represent threshold values corresponding to modern oxic sediment values, concentrations notably below which are indicative of reducing conditions.

The *P. siluricus* conodont zone is also at the base of the section, followed by the *P. latialata–O. snajdri* interval zone and the *Ozarkodina crispa* zone (Figs 5, 6; Lehnert *et al.* 2007; Frýda *et al.* 2021*b*). Based on the vitrinite reflectance of Silurian graptolites in the Prague Basin of 0.78–1.53%, which corresponds to conodont colour alteration index values of 2.5–3.5, burial temperatures likely ranged from 100 to 160°C (Epstein *et al.* 1977; Suchy *et al.* 2002; Hackley and Cardott 2016). Several geochemical aspects of the Lau CIE have been analysed from this section, including continental weathering, palaeoclimate and marine palaeoredox proxies, such as δ^7Li, $\delta^{13}C_{carb}$, $\delta^{13}C_{org}$, $\delta^{18}O_{carb}$, $\delta^{34}S_{pyr}$, $\delta^{34}S_{CAS}$, $^{44/40}Ca$, $^{87}Sr/^{86}Sr$, $\delta^{138}Ba$, $^{187/188}Os$, $\delta^{238}U$ and some trace elements (Lehnert *et al.* 2007; Frýda and Manda 2013; Farkaš *et al.* 2016; Frýda *et al.* 2021*a*, *b*; Sproson *et al.* 2022; Zhang *et al.* 2022; del Rey *et al.* 2023).

The Kosov Quarry section begins with a series of dark brown and grey finely laminated shales, which quickly become interbedded with marly limestone deposits. Within the section, there is an unconformity representative of a stratigraphic gap associated with a flat-pebble

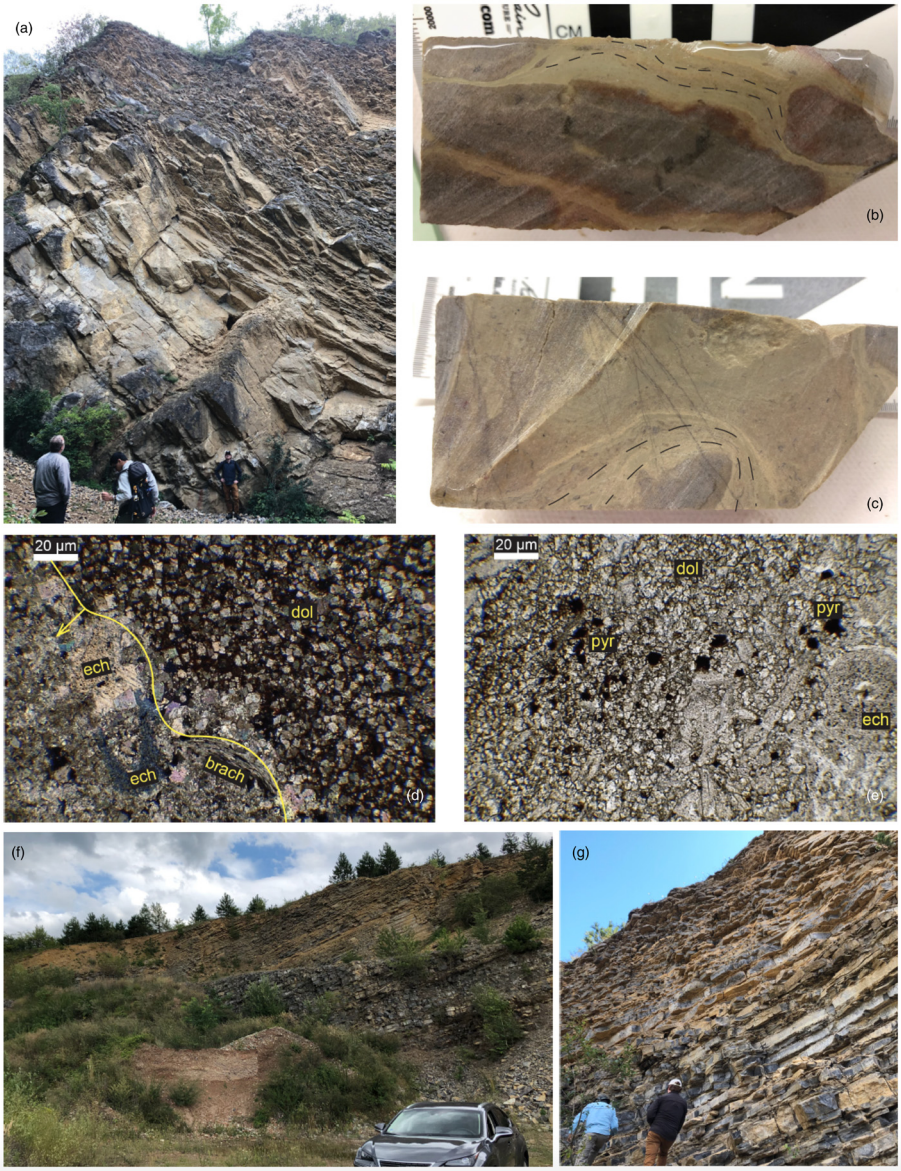

Fig. 3. (**a**) Field photograph of massively to thinly bedded mudstones, wackestones and packstones in the lower portion of the Kopanina Formation exposed in the Mušlovka Quarry section. (**b**, **c**) Hand samples from the flat-pebble conglomerate intervals in the Mušlovka Quarry section. Flat-pebble clasts are purple–grey within a light brown matrix; possible microbial laminations surrounding some flat pebbles are traced by dashed lines. (**d**) Thin section photomicrograph from the Mušlovka Quarry section showing the boundary between a wackestone flat-pebble conglomerate clast and dolomitized matrix, arrow point towards clast (8.5 m). (**e**) Thin section photomicrograph from the Mušlovka Quarry section; example of finely disseminated pyrite in dolomitized matrix (7.5 m, plane light). (**f**) Field photo of upper and lower sections of the interbedded shales and limestones of the Kopanina Formation at Kosov Quarry. (**g**) Field photograph of the upper section at Kosov Quarry showing thinly bedded shale interspersed in more massively bedded carbonates. dol, dolomite; ech, echinoderm fragment; brach, brachiopod; pyr, pyrite.

conglomerate bed. As the section continues, the shale lithology becomes lighter in colour and more calcareous; limestone interbeds also become more numerous. This increase in carbonate content at Kosov Quarry is due to an overall shallowing trend in eustatic sea-level during the glaciation (Lehnert *et al.* 2007; Gocke *et al.* 2013; Frýda *et al.* 2021*b*). The top of the section contains a cephalopod limestone bed, likely deposited during a sea-level lowstand (Ferretti and Kříž 1995), and tuffites are dispersed within the section. The complicated stratigraphy in Kosov Quarry is due to repetitive local sea-level changes combined with increasing accommodation space due to subsidence and carbonate platform destruction during sea-level lowstands (Lehnert *et al.* 2007; Manda *et al.* 2012; Frýda and Manda 2013; Gocke *et al.* 2013; Frýda *et al.* 2021*a*, *b*).

Materials and methods

Sample preparation

Samples were collected and described in *c.* 0.5 m increments through the Kopanina Formation of the Mušlovka Quarry and Kosov Quarry sections in the Prague Basin, Czech Republic (Lehnert *et al.* 2007). Where possible, intervals that were notably weathered or had obvious diagenetic influences (e.g. secondary calcite veins, notable recrystallization, Fe oxide staining or pyrite nodules) were avoided during sampling. For the Mušlovka Quarry carbonate samples, weathered edges and large secondary calcite veins were removed using a water-based diamond blade saw. Representative samples from each section were slabbed for thin section analysis. From each carbonate sample *c.* 1 g of powder was preferentially micro-drilled from the micritic matrix (except in the case of grainstones) for $\delta^{13}C_{carb}$ and I/Ca analyses. For all other geochemical analyses, 200–300 g of sample were crushed and powdered using an alumina ceramic disc mill with a SPEX8510 ShatterBox. The shale samples collected at the Kosov Quarry section were first cleaned via the removal of weathered surfaces using an ultrasonic bath in deionized water. The samples were then crushed using an agate mortar and pestle to produce 7–10 g of powdered rock. Splits of these powders were used for the various geochemical analyses.

Carbon isotopes

For carbonate C isotope analyses, between 0.2 and1 mg of powder was weighed out from each sample. The powders were acidified with 100% H_3PO_4 at 25°C for 24 h. Stable C and O isotopes of the evolved CO_2 gas were then analysed using a ThermoFinnigan Gas Bench II Autocarbonate device coupled to a ThermoFinnigan Delta Plus XP isotope ratio mass spectrometer at the National High

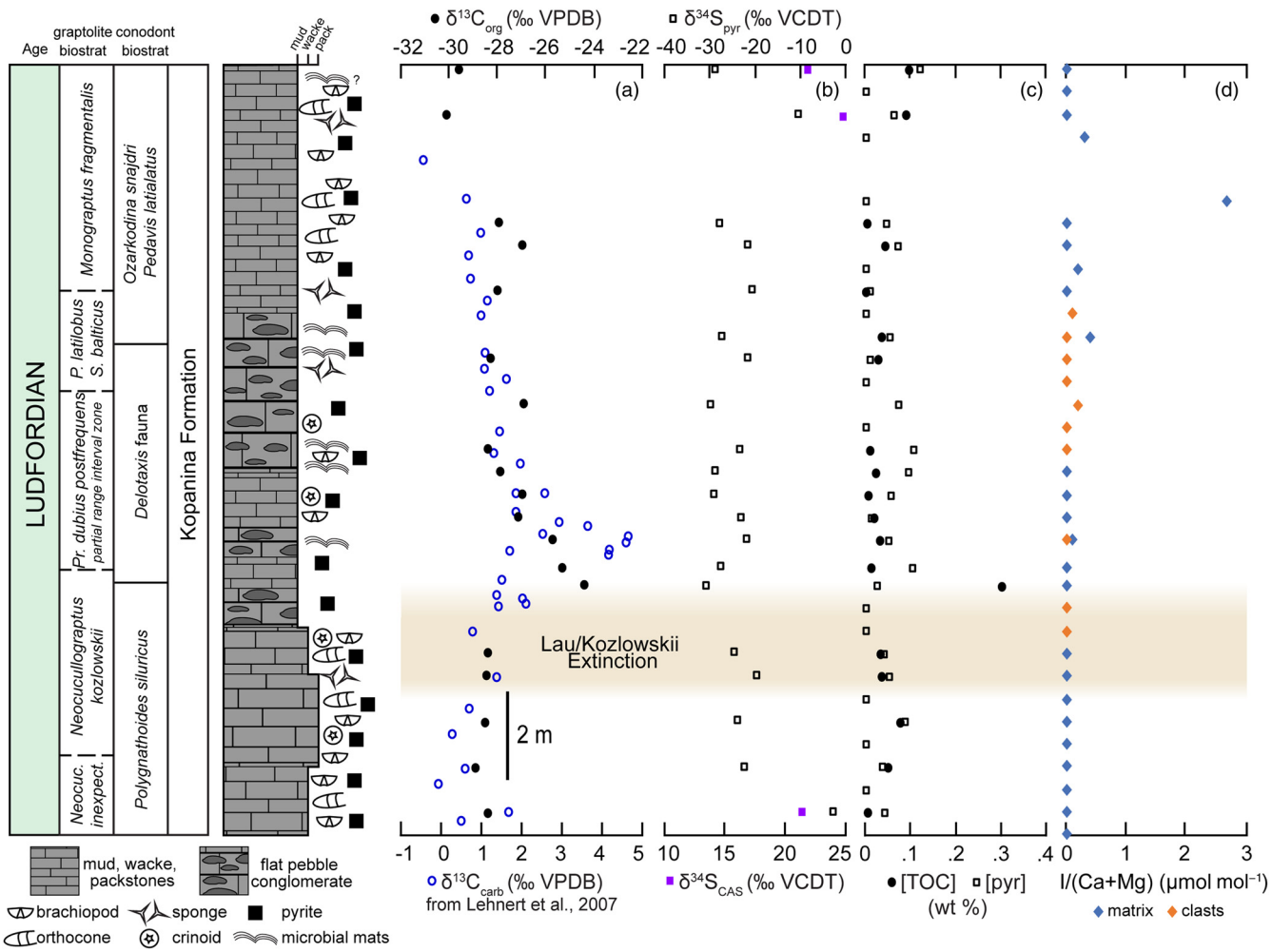

Fig. 4. Stratigraphic column and geochemical data for the Mušlovka Quarry section, Prague, Czech Republic. (**a**) Carbonate and organic C isotope data (carbonate C isotope data from Lehnert *et al.* 2003, 2007). (**b**) Carbonate-associated sulfate and pyrite S isotope data. (**c**) Total organic carbon and pyrite concentration data. (**d**) I/(Ca + Mg) ratio data from both the micritic matrix and flat-pebble conglomerate clasts. The Lau/Kozlowskii extinction is highlighted in tan. Biozonation from Chadimova *et al.* (2015). Carb, carbonate; org, organic; CAS, carbonate-associated sulfate; pyr, pyrite; *Neocuc. inexpect.*, *Neocucullograptus inexpectatus*; *Pr. dubius postfrequens, Prisiograptus dubius postfrequens*; *P. latilobus, Pseudomonoclimacis latilobus*; *S. balticus, Slovenograptus balticus*.

Magnetic Field Laboratory (NHMFL) at Florida State University. The analytical precision of $\delta^{13}C_{carb}$ was ±0.05‰ (1σ) and $\delta^{18}O_{carb}$ was ±0.1‰ (1σ) based on long-term replicate analysis of NBS-19 and other laboratory standards.

Organic C isotope analyses were carried out on a subset of samples from Mušlovka Quarry and all the shale interbeds from Kosov Quarry. Between 2 and 4 g of carbonate or shale powder were accurately weighed and then acidified at least three times with 6 M HCl to remove carbonate minerals. The insoluble residues were then rinsed in ultrapure (deionized, 18.2 MΩ) water until a neutral pH was reached, then dried overnight in an oven at 70°C. The residues from each sample were homogenized in agate mortars and weighed into tin cups for analysis. The organic C isotope values were measured using a Costech Elemental Analyzer coupled to a ThermoFinnigan Delta Plus XP isotope ratio mass spectrometer via an open-split Conflo III at the NHMFL. The weight per cent of total organic carbon (TOC) was determined by comparison of the voltages for the ion beam intensities of masses 44, 45 and 46 for CO_2^+ between our samples and known weight per cent carbon of the gravimetric standard acetanilide. The analytical precisions of ±0.2‰ (1σ) for $\delta^{13}C_{org}$ and ±0.7% (1σ) for %C are based on long-term replicate analysis of laboratory standards calibrated to International Atomic Energy Agency standards. All the C isotope data are reported in standard delta notation (δ) with units of per mil (‰) relative to the Vienna Pee Dee Belemnite (VPDB) standard.

Sulfur isotopes

Carbonate-associated sulfate (CAS) extractions for S isotope analysis were performed on the carbonate samples from Mušlovka Quarry with minor modifications from procedures outlined by Wotte *et al.* (2012). For each sample, between 80 and 250 g of powdered carbonate were rinsed three times in a 10% NaCl solution and three times in ultrapure (deionized, 18.2 MΩ) water for *c.* 12 h per rinse to remove soluble secondary sulfate minerals (Edwards *et al.* 2019). The samples were then acidified through titration with 6 M HCl for no more than 2 h per sample in an attempt to avoid pyrite oxidation. The insoluble residues were then separated from the acidified solutions via centrifugation. The acidified solutions were brought up to a pH of 10 with NaOH and the precipitates from this reaction were removed through vacuum filtration. Post-filtration, the remaining solutions were re-acidified to pH 4 using a few drops of 12 M HNO_3. Excess $BaCl_2$ was added to each sample solution and dissolved sulfate was allowed to precipitate as barite ($BaSO_4$) over 72 h. The barite was then rinsed in ultrapure water and dried.

Cr-reducible sulfides were extracted from the insoluble residues remaining from the CAS extraction of the Mušlovka Quarry samples and from the powdered Kosov Quarry samples based on modified protocols from Canfield *et al.* (1986) and Brüchert and Pratt (1996). The residues were reacted with a 70:30 mixture of 12 M HCl and 1 M $CrCl_3$ in an N_2-purged flask. The evolved H_2S gas was then

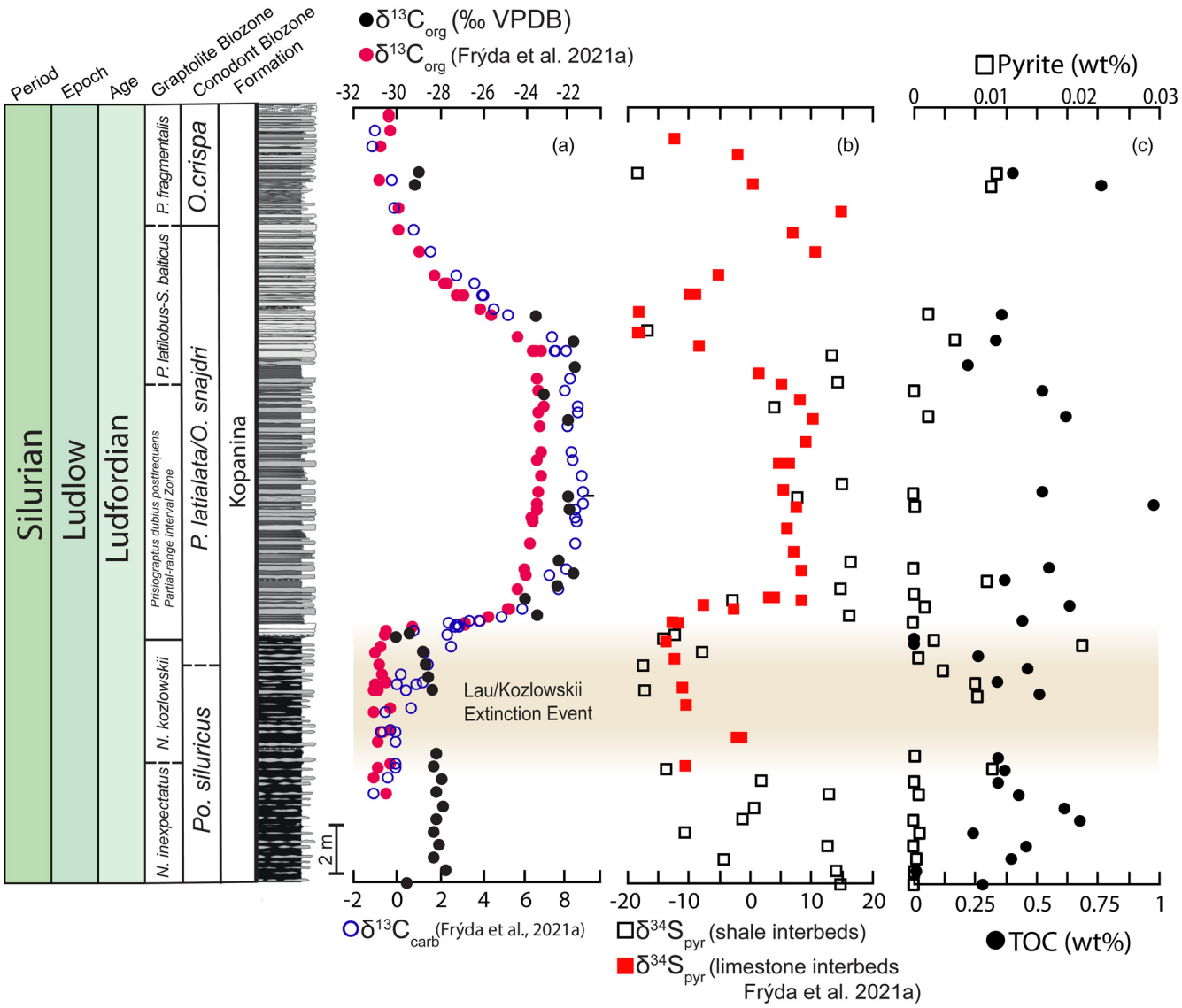

Fig. 5. Stratigraphic column and geochemical data for the Kosov Quarry section, Beroun, Czech Republic. (**a**) Organic C isotope data (additional carbonate and organic C isotope data from Frýda *et al.* 2021*a*). (**b**) Pyrite S isotope data (additional data from Frýda *et al.* 2021*a*). (**c**) Total organic carbon concentration data. The Lau/Kozlowskii extinction is highlighted in tan. Carb, carbonate; org, organic; pyr, pyrite; TOC, total organic carbon; *N. inexpectatus*, *Neocucullograptus inexpectatus*; *N. kozlowskii*, *Neocucullograptus kozlowskii*; *P. latilobus*, *Pseudomonoclimacis latilobus*; *S. balticus*, *Slovenograptus balticus*; *P. fragmentalis*, *Pristiograptus fragmentalis*; *Po. siluricus*, *Polygnathoides siluricus*; *O. snajdri*, *Ozarkodina snajdri*; *P. latialata*, *Pedavis latialata*; *O. crispa*, *Ozarkodina crispa*.

bubbled into $AgNO_3$ to precipitate Ag_2S. The total amount of precipitant was gravimetrically determined to calculate the concentration of pyrite in each sample, assuming quantitative stoichiometry. About 350 µg of barite (CAS) or silver sulfide (Cr-reducible sulfides) were weighed into tin cups with excess V_2O_5 for S isotope analysis using a Thermo Isolink Elemental Analyzer coupled via an open-split Conflo IV to a Thermo Delta V Plus isotope ratio mass spectrometer at the NHMFL. All the S isotope results are reported in standard delta notation (δ) with units of per mil (‰) relative to the Vienna Cañon Diablo Troilite (VCDT) standard. Analytical precision is ±0.2‰ (1σ) based on long-term replicate analysis of the International Atomic Energy Agency S-3 standard and calibrated internal laboratory standards.

Iodine-to-calcium ratios

The I/(Ca + Mg) ratios, hereafter referred to as I/Ca, were measured for the Mušlovka Quarry samples at the NHMFL using an Agilent 7500 cs quadrupole inductively coupled plasma mass spectrometer according to standard methods (e.g. Z. Lu *et al.* 2010; W. Lu *et al.* 2017 ; Hardisty *et al.* 2014, 2017). About 2–5 mg of micro-drilled carbonate powder were acidified with 3% HNO_3 to dissolve all carbonate material. The samples were vortexed and centrifuged to ensure the complete dissolution of carbonate and separation from the insoluble residue. The supernatant was then diluted to a *c.* 50 ppm Ca + Mg solution in a matrix of 2% HNO_3. The samples were re-run until a consistent matrix of 50 ppm ± 5 ppm Ca + Mg was achieved. Calibration standards were made each day by serial dilution of a 10 ppm iodine inductively coupled plasma mass spectrometry standard from High Purity Standards with a similar matrix of *c.* 50 ppm Ca + Mg. Analyses were performed on the inductively coupled plasma mass spectrometer at the NHMFL within 2 h of acidification (due to the volatility of iodine).

The precision of the ^{127}I results was typically better than 2% and is not reported separately for individual samples. Standard deviation in counts per second (cps) for three blanks in a row was typically below 300 cps and the sensitivity for a 1 ppb standard was typically 60 000–120 000 cps depending on the instrumental set-up each day (i.e. the sensitivity varies day-to-day, but the geostandards

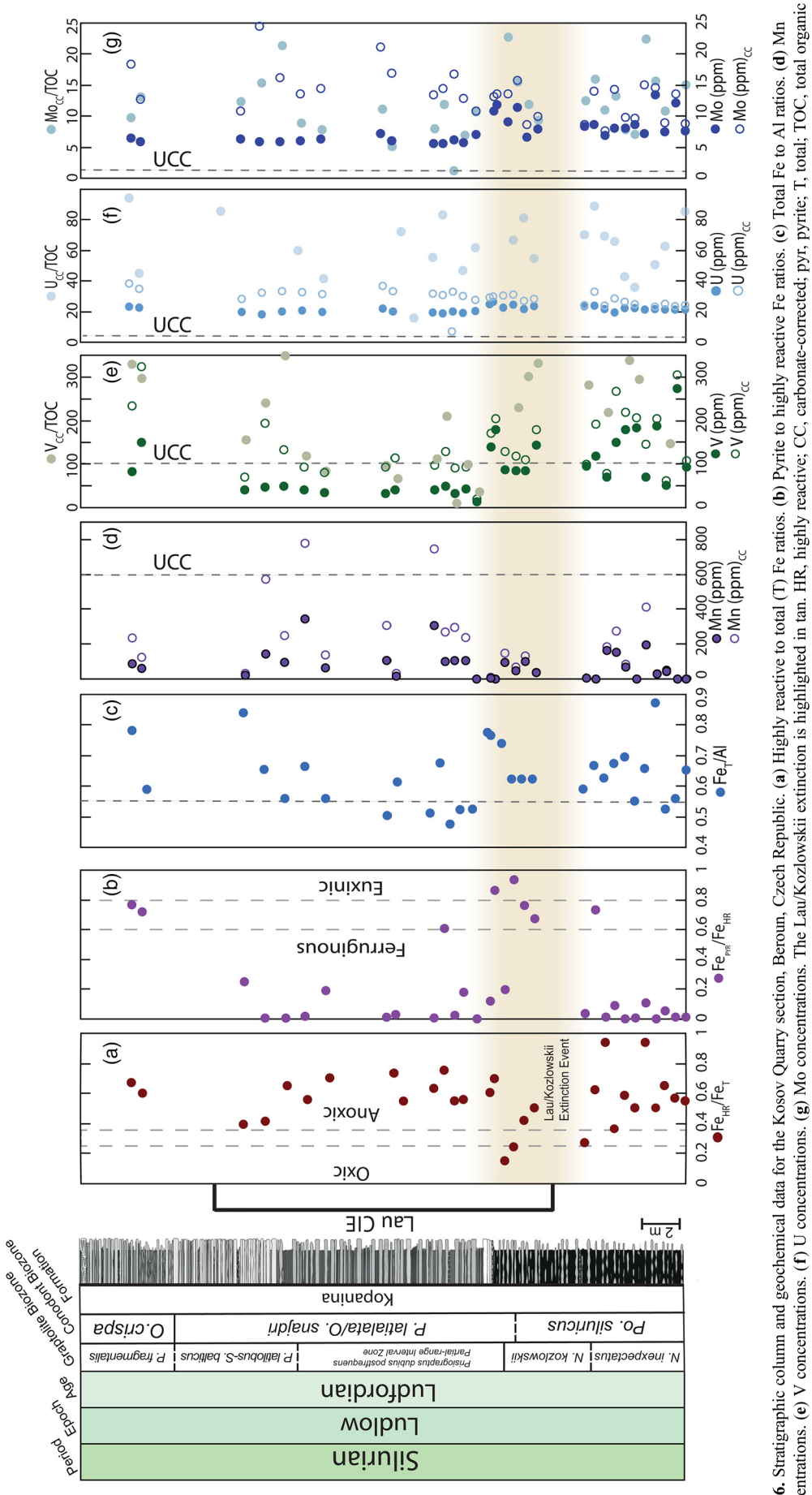

Fig. 6. Stratigraphic column and geochemical data for the Kosov Quarry section, Beroun, Czech Republic. (**a**) Highly reactive to total (T) Fe ratios. (**b**) Pyrite to highly reactive Fe ratios. (**c**) Total Fe to Al ratios. (**d**) Mn concentrations. (**e**) V concentrations. (**f**) U concentrations. (**g**) Mo concentrations. The Lau/Kozlowskii extinction is highlighted in tan. HR, highly reactive; CC, carbonate-corrected; pyr, pyrite; T, total; TOC, total organic carbon; UCC, upper continental crust; see Figure 5 caption for graptolite and conodont biozones.

document consistent ratios).The long-term accuracy of this procedure was based on replicate analysis of internal FSU–NHMFL laboratory reference materials KL 1–2 (±0.50 µmol mol^{-1}) and KL 1–4 (±0.46 µmol mol^{-1}) based on Hardisty *et al.* (2014) and previous work from the Geochemistry Group at the NHMFL (Lowrey *et al.* 2018; Bowman *et al.* 2020; Kozik *et al.* 2022; Lindskog *et al.* 2023). I/Ca ratios. The notation used throughout are commonly reported as I/(Ca + Mg) to account for the variable carbonate mineralogy and particularly dolomitization in ancient carbonates (e.g. Hardisty *et al.* 2014, 2017; W. Lu *et al.* 2017, 2018).

Iron geochemistry

Based on the methods outlined in Poulton and Canfield (2005), *c.* 100 mg of powdered rock from each of the Kosov Quarry shale samples were weighed into 15-mL centrifuge tubes. The interbedded carbonates were not analysed. A solution of 1 M sodium acetate was buffered to a pH of 4.5 to extract the Fe associated with the carbonate phases (Fe_{carb}). A 10-mL volume of sodium acetate was added to each sample, which was then placed on a shaker table for 24 h. The next extraction process removed the Fe associated with crystalline oxides (Fe_{ox}) by adding 0.29 M sodium dithionite buffered with 0.35 M acetic acid and 0.2 M sodium citrate to each sample, which were then agitated for 2 h. Fe-in-magnetite (Fe_{mag}) was selectively extracted by the addition of 0.2 M ammonium oxalate and 0.17 M oxalic acid buffered to pH 3.2 to each sample and then shaking for 6 h. An aliquot of the supernatant was saved from each extraction step, diluted with 2% HNO_3, and analysed on the Agilent 7500 cs quadrupole inductively coupled plasma mass spectrometer at the NHMFL. Highly reactive Fe (Fe_{HR}) was calculated by summing $Fe_{carb} + Fe_{ox} + Fe_{mag} + Fe_{pyr}$. The sequential Fe method has a reproducibility of *c.*±7%. Fe_{pyr} was determined by weighing the Ag_2S precipitate from Cr-reducible sulfide extraction and then quantitative stoichiometry was used to calculate Fe_{pyr}.

Major and trace element geochemistry

A multistep acid digestion procedure was used to dissolve each of the powdered shales from the Kosov Quarry; importantly, the interbedded carbonates were not analysed. Powdered samples were weighed into Teflon beakers and then digested in various combinations of concentrated HNO_3, HCl and HF that were free of trace metals. The samples were kept on hot-plates at *c.* 120–160°C, typically overnight, then dried each time before a new acid solution was added. H_2O_2 that was free of trace metals was used to oxidize the organic matter when necessary. After complete dissolution, the samples were dried and re-dissolved in 2% HNO_3 before being diluted and analysed for major and trace element concentrations at the NHMFL using an Agilent 7500 cs quadrupole inductively coupled plasma mass spectrometer. USGS standards SDO-1, SCO-1 and SGR-1 were dissolved along with the samples and were within the analytical ranges for the reported elements. The results are reported in ppm with an analytical precision of ±5% or better for Fe, Al, Mn, V, U and Mo. The blanks were below the detection limit.

The trace element results are plotted as absolute concentrations, carbonate-corrected concentrations and TOC-normalized concentrations (Fig. 6). The Mn concentrations are reported and discussed in the text as carbonate-corrected values; V, U and Mo are reported and discussed as carbonate-corrected values normalized to each sample's TOC content. We also present enrichment factor data for U and Mo (Fig. 7). Trace metal enrichment factors are calculated as $X_{EF} = [(X/Al)_{sample}/(X/Al)_{PAAS}]$, where X is the concentration in each sample of the element in question (here either U or Mo) and Al is the concentration of Al in the sample. The quotient of X/Al_{sample} is then normalized to the ratio of X/Al in post-Archean average shale (Taylor and McLennan 1995). Samples with values >3 are considered to have detectable authigenic enrichment and values >10 have substantial enrichment (Algeo and Tribovillard 2009).

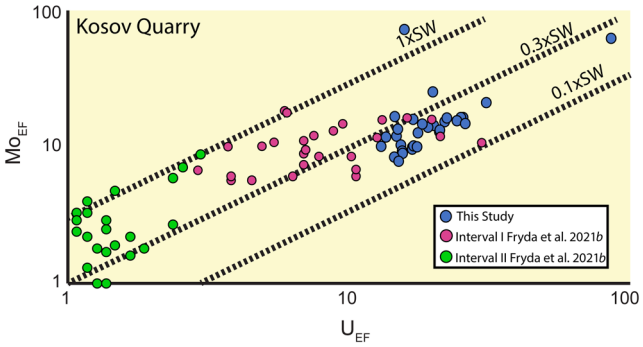

Fig. 7. Cross-plot of U and Mo enrichment factors for Kosov Quarry based on plots from Algeo and Tribovillard (2009). Blue symbols show data from this study, green symbols show corresponding data from Frýda *et al.* (2021*b*). Diagonal dashed lines represent seawater Mo/U ratio of *c.* 7.5–7.9 and fractions thereof. SW, seawater.

Results

Mušlovka Quarry sedimentological and geochemical results

The Lau CIE has been previously documented in the Mušlovka Quarry section by Lehnert *et al.* (2003, 2007) as a *c.* +5‰ magnitude excursion in $\delta^{13}C_{carb}$ just above the *N. kozlowskii* zone. Here, we document a roughly parallel excursion in $\delta^{13}C_{org}$ *c.* +4.2‰ in magnitude (Fig. 4a, black symbols). Pre-excursion baseline values of *c.* −28.5‰ in $\delta^{13}C_{org}$ quickly rose to a peak of −24.3‰ just above the last appearance datum *of P. siluricus* and before the peak in $\delta^{13}C_{carb}$ values. Subsequently, the $\delta^{13}C_{org}$ values steadily decreased to a post-excursion baseline of *c.* −29‰. The I/Ca ratios were low throughout the section, consistently between 0 and 0.4 µmol mol^{-1} in both the carbonate mud matrix and in flat-pebble conglomerate clasts (Fig. 4d). There was one higher value of 2.7 µmol mol^{-1} recorded from the upper part of the section within the *M. fragmentalis* graptolite zone. The $\delta^{34}S_{CAS}$ data were sparse due to the overall high concentrations of pyrite within this succession, with values only from the *N. inexpectatus* and *M. fragmentalis* graptolite zones, which ranged from +21.5 to +24.8‰ (Fig. 4b, purple symbols). The $\delta^{34}S_{pyr}$ values were relatively constant throughout the Mušlovka Quarry section, ranging from −30.6 to −20.3‰ with a slight negative trend moving upwards through the section (Fig. 4b, black symbols).

Kosov Quarry sedimentological and geochemical results

The Lau CIE has been previously documented in the Kosov Quarry section by Lehnert *et al.* (2007), Frýda and Manda (2013) and Frýda *et al.* (2021*a*) as a *c.* +8‰ magnitude excursion in $\delta^{13}C_{carb}$ in the *P. dubius postfrequens* partial range interval and the combined *M. latilobus–S. balticus* graptolite zones just above the *N. kozlowskii* zone (Fig. 5a). Frýda *et al.* (2021*a*) also reported a *c.* +7‰ magnitude excursion in $\delta^{13}C_{org}$ through the same stratigraphic interval. The $\delta^{13}C_{org}$ data collected from the Kosov Quarry shale interbed samples for the present study begin at pre-excursion baseline values of *c.* −30‰ during the *M. inexpectatus* and *N. kozlowskii* graptolite biozones (Fig. 5a). Much of the rising limb of the excursion is missing/condensed due to an absence of shale in a short interval from *c.* 50 to 80 cm above the top of the *N. kozlowskii* biozone. Subsequently, higher in the section shale, interbeds are

once more present in the *P. dubius postfrequens* graptolite zone; their corresponding $\delta^{13}C_{org}$ values range from −24‰ to −22‰ in the peak interval of the Lau CIE. Around 20 m above the base of the section, the $\delta^{13}C_{org}$ values gradually begin to fall back to a post-excursion baseline of −30‰ during the combined *M. latiobus–S. balticus* then *M. fragmentalis* graptolite zones. Newly gathered $\delta^{13}C_{org}$ data fit well with the stratigraphically high-resolution $\delta^{13}C_{org}$ record reported by Frýda *et al.* (2021*a*).

The $\delta^{34}S_{pyr}$ data from the shale interbeds generally co-vary with the C isotope datasets generated from the Kosov Quarry. As with the C isotope data, the $\delta^{34}S_{pyr}$ values from our Kosov Quarry shale samples are plotted along with $\delta^{34}S_{pyr}$ values generated from the limestone interbeds of this section from Frýda *et al.* (2021*a*). The shale $\delta^{34}S_{pyr}$ data from the base of the measured section show a wide range of values from −20‰ to +15‰ (Fig. 5b, red symbols). In general, the data from the shale interbeds are comparable with those of the limestone interbeds, despite the slightly wider range in isotope values. Within the upper *N. kozlowskii* graptolite zone, $\delta^{34}S_{pyr}$ values fall to *c.* −15‰. Near the end of the LKE interval, in the lower *P. dubius postfrequens* graptolite zone, the $\delta^{34}S_{pyr}$ values increase to as much as +15‰ (compared with +7–8‰ in the limestone interbeds; Frýda *et al.* 2021*a*) and stay near this value throughout the interval of peak values of the Lau CIE. After this peak in $\delta^{34}S_{pyr}$, in the *M. latiobus–S. balticus* then *M. fragmentalis* graptolite zones, the values sharply drop back to the −15‰ pre-excursion value. The $\delta^{34}S_{pyr}$ data from the limestone interbeds (Frýda *et al.* 2021*a*) document an additional excursion of *c.* +30‰ across the *M. latilobus–S. balticus* and *M. fragmentalis* graptolite zones that was not captured in our shale interbed dataset (Fig. 5b, red symbols).

The Fe_{HR}/Fe_T values ranged from 0.15 to 0.94 throughout the Kosov Quarry section, with most values >0.38 (Fig. 6a). The Fe_{pyr}/Fe_{HR} values were generally low throughout the section, ranging from 0 to 0.3. Just before and during the LKE extinction, from the upper *M. inexpectatus* zone to the lower *P. dubius postfrequens* zone, the Fe_{pyr}/Fe_{HR} values were notably higher between 0.61 and 0.93 (Fig. 6b). The Fe_T/Al ratios ranged from 0.47 to 0.87 throughout the Kosov Quarry section (Fig. 6c). The values ranged between 0.5 and 0.7 during the *M. inexpectatus* and *N. kozlowskii* zones, then increased to 0.8 during the lower *P. dubius postfrequens* graptolite zone. The values decreased to 0.5–0.7 through the middle and upper *P. dubius postfrequens* graptolite zone before increasing to 0.9 in the *M. latilobus–S. balticus* zone.

The Mn concentrations were relatively low and consistent; most values were <400 ppm, with a few data points near 750 ppm (Fig. 6d). The TOC-normalized V concentrations were somewhat scattered, particularly in the lowest 10 m of the section in the *M. inexpectatus* and *N. kozlowskii* zones (Fig. 6e). At *c.* 10 m, just above the upper boundary of the *N. kozlowskii* zone, there was a decrease in the average V/TOC from *c.* 340 to *c.* 160 ppm/wt%. The U/TOC values through the Kosov Quarry show less scatter than the V/TOC values and there is a slight decrease in the average values just above the upper boundary of the *N. kozlowskii* zone from 73 to 66 ppm/wt% (Fig. 6f). The U_{EF} values range from 13 to 92 with an average value of 22 (Fig. 7). The Mo/TOC values ranged between 10 and 45 ppm/wt% (Fig. 6g). The average Mo/TOC values decreased mid-LKE, in the same interval as V and U, from 27 to 20 ppm/wt% (Fig. 6g). The Mo_{EF} values ranged from 8 to 68 with an average value of 16 (Fig. 7; see also: Supplemental Data Tables).

Discussion

Effects of diagenesis on primary carbonate geochemical signatures at Mušlovka Quarry

All sedimentary strata experience some variety of post-depositional processes that have the potential to alter the primary sedimentary textures and geochemical signatures, complicating the interpretation of proxy data. Carbonate rocks are particularly susceptible to potential diagenetic alteration due to processes such as recrystallization. Many of the samples in the Mušlovka Quarry section show signs of obvious late diagenetic influences in thin section. From 3.0 to 13.0 m in the sampled interval, almost all of the (presumably) once micritic matrix has been dolomitized (Fig. 3d, e). To a lesser extent, the coarser grained components, such as the grainstone to wackestone flat-pebble conglomerate clasts, have also been partially dolomitized (Fig. 3d). The common occurrence of secondary calcite veins, steinkerns and partially recrystallized fossil allochems, and pressure dissolution features such as stylolites, throughout the Mušlovka Quarry section are reflective of this section's complex tectonic and burial history.

General carbonate microfacies analysis of the Mušlovka Quarry section show that diagenetic processes notably affected the primary carbonate textures. Conodont colour alteration indices of 2.5–3.5 in the Mušlovka Quarry section indicate a significant thermal influence on the studied strata (Epstein *et al.* 1977). Regardless, as with any carbonates, it is still important to assess whether the geochemical trends in this study are reflective of primary seawater conditions or are the result of post-burial processes, diagenetic or otherwise (e.g. Banner and Hanson 1990; Railsback *et al.* 2003; Gill *et al.* 2008).

Here, we use geochemical data to assess carbonate diagenetic alteration. First, we use the linear relationships observed in cross-plots of geochemical proxy data, which have been extensively used to assess the degree of diagenetic alteration that sediments or rocks have experienced since deposition (Fig. 8, orange symbols; e.g. Lohmann 1988; Hurtgen *et al.* 2002; Cramer and Saltzman 2005; Swart and Eberli 2005; Gill *et al.* 2008; Jones and Fike 2013). Then we compare our data with modelled diagenetic changes in carbonate proxies based on recent work by Lau and Hardisty (2022). This includes modelled diagenetic changes under sediment- and fluid-buffered meteoric water, oxidizing seawater and reducing seawater (Fig. 8a–c, e and f).

A notable correlation between $\delta^{13}C_{carb}$ and $\delta^{18}O_{carb}$ commonly indicates the partial resetting of C and O isotope values from meteoric fluid flow. A cross-plot of our $\delta^{13}C_{carb}$ and $\delta^{18}O_{carb}$ data (Fig. 8a) shows moderate correlation at Mušlovka Quarry, with an R^2 value of 0.51. This is further supported by comparing the data from the Mušlovka Quarry with the modelled results of meteoric diagenesis in $\delta^{13}C_{carb}$–$\delta^{18}O_{carb}$ space from Lau and Hardisty (2022). Meteoric diagenesis tends to drive both $\delta^{13}C_{carb}$ and $\delta^{18}O_{carb}$ to more isotopically negative values than their starting compositions. This can be clearly seen in the Mušlovka Quarry data, which overlaps with the modelled isotopic changes from meteoric diagenesis (Fig. 8a).

Most of the I/Ca values from the Mušlovka Quarry section are at or near zero (i.e. below detection limit) and, as a result, the linear correlations are not particularly useful for assessing the effects of diagenesis on this proxy (Fig. 8b, c). The low I/Ca values could be indicative of diagenetic resetting due to the recrystallization of the original materials under the flow of reducing pore fluids. The I/Ca proxy has previously been shown to be very sensitive to diagenetic overprinting, which always shifts I/Ca ratios to lower values (e.g. Hardisty *et al.* 2017). Given the clear signal of meteoric diagenesis from $\delta^{13}C_{carb}$ and $\delta^{18}O_{carb}$ and the locally reducing conditions along the palaeomargin, it is difficult to assess whether the low I/Ca values are strictly due to diagenetic overprinting, a primary seawater signal of a low oxygen content in the late Silurian water column, or some combination of these two factors (Hardisty *et al.* 2017). Thus, our data are compared with modelled diagenetic changes in I/Ca relative to both $\delta^{13}C_{carb}$ and $\delta^{18}O_{carb}$ (Fig. 8b, c; Lau and Hardisty 2022).

As a result of the overlap in signals produced from modelling meteoric and reducing seawater fluid-buffered diagenetic changes

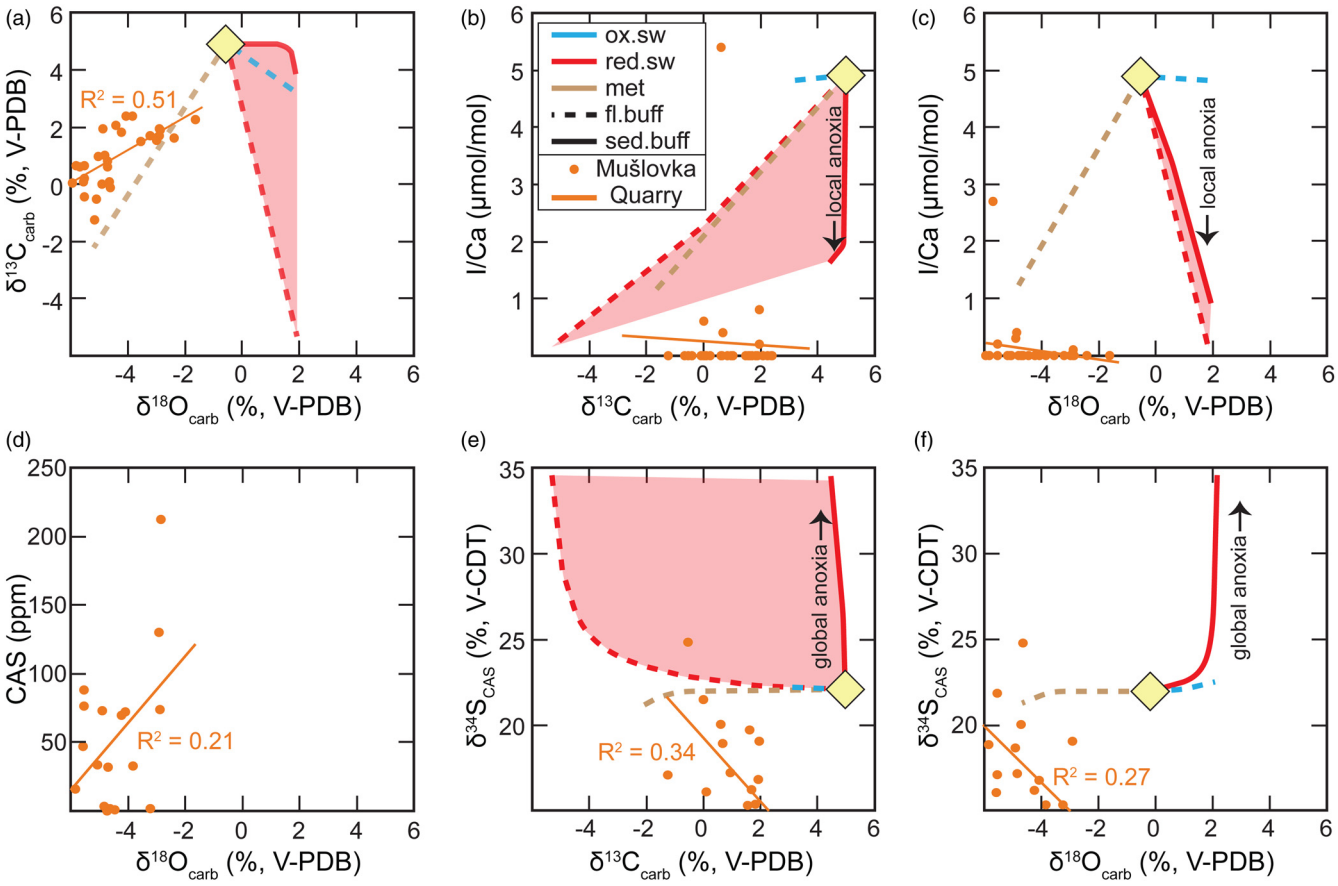

Fig. 8. Cross-plots for the assessment of possible diagenetic alteration of C, O and S isotopes and I/Ca values in the Mušlovka Quarry shallow shelf carbonate section. (**a**) $\delta^{18}O_{carb}$ v. $\delta^{13}C_{carb}$. (**b**) $\delta^{13}C_{carb}$ v. I/Ca. (**c**) $\delta^{18}O_{carb}$ v. I/Ca. (**d**) $\delta^{18}O_{carb}$ v. [CAS]. (**e**) $\delta^{13}C_{carb}$ v. $\delta^{34}S_{CAS}$. (**f**) $\delta^{18}O_{carb}$ v. $\delta^{34}S_{CAS}$. Modelling results from Lau and Hardisty (2022) are also presented in most panels, showing changes in C, O and S isotopes and I/Ca values based on varying diagenetic conditions. The yellow diamond represents the starting composition in the model. The lines represent sediment-buffered (solid) and fluid-buffered (dashed) conditions for diagenesis with meteoric water (brown), reducing seawater (red) and oxic seawater (blue). Arrows represent traditional interpretations for redox proxies in the absence of diagenetic overprinting.

in I/Ca–$\delta^{13}C_{carb}$ space, the cause of the low I/Ca values in the Mušlovka Quarry data remains unclear. When compared with the Lau and Hardisty (2022) modelling results in I/Ca–$\delta^{18}O_{carb}$ space, however, the more negative $\delta^{18}O_{carb}$ data from Mušlovka Quarry again suggest that meteoric diagenesis played a part in the extremely low I/Ca values (Fig. 8c). Beyond the comparison of our data with the modelled diagenetic effects on carbonate processes, the one data point at Mušlovka Quarry that was significantly above the detection limit (2.7 µmol mol^{-1}) is located stratigraphically above the heavily dolomitized interval within this succession, further supporting the hypothesis that diagenetic influences had almost no effect on the I/Ca values throughout most of the section.

The concentration of sulfate in the carbonate crystal lattice has also been shown to decrease during alteration because meteoric fluids have lower concentrations of both sulfate and iodate than the original calcite (Gill *et al.* 2008; Sim *et al.* 2015; Hardisty *et al.* 2017). The flow of meteoric fluids – and likely the flow of other diagenetic fluids –although known to decrease CAS concentrations, have little effect on the $\delta^{34}S_{CAS}$ values (Gill *et al.* 2008; Sim *et al.* 2015; Lau and Hardisty 2022). There is a weak correlation between $\delta^{18}O_{carb}$ and [CAS] in the Mušlovka Quarry section, with $R^2 = 0.21$ (Fig. 8d). However, it should be noted that most of the [CAS] are <100 ppm, suggesting significant diagenetic alteration. Correlations between $\delta^{13}C_{carb}$ and $\delta^{34}S_{CAS}$ and between $\delta^{18}O_{carb}$ and $\delta^{34}S_{CAS}$ are of minor to perhaps moderate significance at the Mušlovka Quarry section, with R^2 values of 0.34 and 0.27, respectively (Fig. 8e, f). When assessed in relation to the Lau and Hardisty (2022) diagenetic models, the $\delta^{34}S_{CAS}$ data plots outside the fields related to diagenetic activity. The effects of meteoric diagenesis are still seen in the relatively low isotopic values of $\delta^{13}C_{carb}$ and $\delta^{18}O_{carb}$. However, as stated previously, meteoric diagenesis has very little effect on $\delta^{34}S_{CAS}$, which plays out in the near-horizontal dashed brown lines in the $\delta^{13}C_{carb}$–$\delta^{34}S_{CAS}$ and $\delta^{18}O_{carb}$–$\delta^{34}S_{CAS}$ model space (Lau and Hardisty 2022).

The $\delta^{34}S_{CAS}$ values at the Mušlovka Quarry section are noticeably lower than what seem to be baseline Ludfordian seawater values of *c.* +24‰. This is based on pre- and post-excursion baseline $\delta^{34}S_{CAS}$ values from multiple sections on the southern Laurentian margin (Bowman *et al.* 2020). As such, the $\delta^{34}S_{CAS}$ values from the Mušlovka Quarry section that were isotopically lighter than a conservative value of +20‰ (values between +11.7 and +19.7‰; see Supplemental Data Tables) were discarded as not being representative of primary Ludfordian seawater and most likely contaminated by the oxidation of sedimentary pyrite during laboratory CAS extraction. This is likely to be attributable to the ubiquitous presence of pyrite within the Mušlovka Quarry section. High pyrite concentrations such as these complicate the CAS laboratory extraction process; the higher the pyrite concentration, the more likely it is to be oxidized during the acidification of powdered carbonate samples (e.g. Present *et al.* 2015; Edwards *et al.* 2019; Richardson *et al.* 2019).

A slight correlation ($R^2 = 0.24$) between $\delta^{34}S_{CAS}$ and $\delta^{34}S_{pyr}$ shows that when the pyrite sulfur values were isotopically lighter, the CAS values also tended to be lighter (see Supplemental Data Tables). However, it is also possible that the variability in the Ludfordian $\delta^{34}S_{CAS}$ values is due to regional heterogeneity in the

seawater sulfate pool resulting from low seawater sulfate concentrations. Relatively low seawater sulfate concentrations have also been suggested to contribute to small offsets in excursion magnitudes and baseline values between $\delta^{34}S_{CAS}$ datasets for the late Cambrian Steptoean positive C isotope excursion (SPICE; Gill *et al.* 2011*b*) and the mid-Silurian Ireviken event (Young *et al.* 2019). Recent S isotope mass balance modelling by Zhang *et al.* (2022) also supports the possibility of low seawater sulfate concentrations during the Ludfordian. Based on their model results, concentrations may have been as low as 1.1–1.2 mM in the late Silurian oceans (compared with 28 mM in the modern ocean; Zhang *et al.* 2022).

Local redox of the shallow shelf

The I/Ca values were low (0–0.4 μmol mol^{-1}) throughout the Mušlovka Quarry section and showed no systematic variation between the carbonate matrix and clasts within the flat-pebble conglomerate intervals (Fig. 4d). This could be the result of consistently low or no oxygen in the water column or adjacent water masses (e.g. Z. Lu *et al.* 2010; W. Lu *et al.* 2018). I/Ca analyses typically target the micritic matrix and, in the case of Mušlovka Quarry, much of what was once micritic matrix has been heavily dolomitized, with even skeletal grains showing partial recrystallization (Fig. 3d, e). Importantly, the one I/Ca value notably above the detection limit (*c.* 2.7 μmol mol^{-1}) is stratigraphically above the dolomitized interval. Given the complex tectonic history and the clear signal of meteoric diagenesis, it is unlikely that the I/Ca values from Mušlovka are a primary seawater signature (Lau and Hardisty 2022).

Notable positive excursions in $\delta^{34}S_{CAS}$ have been documented in the shallow tropical seas of both Laurentia and Baltica, with magnitudes between +8 and +30‰, recording the enhanced burial and preservation of pyrite across the global ocean (Bowman *et al.* 2019, 2020). Again, in sections from Laurentia and Baltica, this is accompanied by parallel positive excursions in $\delta^{34}S_{pyr}$, with magnitudes between +20 and +68‰, which mirror this signal of enhanced pyrite burial on a local to regional scale. At Mušlovka Quarry, no positive excursion was recorded that suggested the record of $\delta^{34}S_{pyr}$ is reflective of the global changes in S isotopes of seawater sulfate that have been recorded on the southern Laurentian margin and in the Baltic Basin (Bowman *et al.* 2019, 2020). Thus, it is likely that the $\delta^{34}S_{pyr}$ values are representative of local factors, such as rate of microbial sulfate reduction (MSR), sulfate concentrations, the availability of organic matter or Fe, changes in the location of pyrite formation, changes in sedimentation rates and/or changes in sea-level (e.g. Canfield and Thamdrup 1994; Leavitt *et al.* 2013; Gomes and Hurtgen 2015; Kozłowski 2015; Farkaš *et al.* 2016; Sim 2019; Pasquier *et al.* 2021).

The isotopic difference ($\Delta^{34}S$) between marine sulfate ($\delta^{34}S_{CAS}$) and sedimentary pyrite ($\delta^{34}S_{pyr}$) can be indicative of the locus of pyrite formation in the water column and/or sediment porewaters and its formation via open- or closed-system MSR (Gomes and Hurtgen 2015). Based on the limited $\delta^{34}S_{CAS}$ data at Mušlovka Quarry (Fig. 4b), lower $\Delta^{34}S$ values of *c.* 24‰ (due to higher $\delta^{34}S_{pyr}$) in the lower part of the section, the *N. inexpectatus* zone, could be indicative of pyrite formation via more closed-system MSR within sediment porewaters. Higher $\Delta^{34}S$ values of 35–50‰ in the upper part of the section (*M. fragmentalis* zone) imply that pyrite formed via more open-system MSR, either in the water column or at the sediment–water interface (Gomes and Hurtgen 2015).

Although our $\delta^{34}S_{pyr}$ data are not reflective of the global enhancement of pyrite burial during the mid-Ludfordian, pyrite concentrations in the Mušlovka Quarry carbonate succession were high throughout the section, with sedimentary pyrite being observed in both hand sample and thin section (Fig. 4c). Pyrite concentrations averaged *c.* 600 ppm and were as high as 1200 ppm in the upper part of the section (Fig. 3c), suggesting at the very least that the sediment porewaters in the shallow shelf of the Prague Basin were reducing and likely sulfidic (Fig. 9). The low I/Ca values, the prevalence of finely disseminated pyrite through the measured section and the high $\Delta^{34}S$ values all support the possibility of reducing bottom water and sediment porewater conditions at the site of the shallow shelf deposition of the Mušlovka Quarry section.

Local redox of the deep shelf

The Fe speciation and trace element concentrations from mid-Ludfordian successions have been documented previously in the deep shelf shales and mudstones of the tropical Baltic Basin and Richardson Trough (Bowman *et al.* 2021; Sperling *et al.* 2021) and the mid-latitudes of peri-Gondwana (Frýda *et al.* 2021*b*). At Kosov Quarry, in the deep shelf section of the Prague Basin, the ratios of highly reactive to total Fe (Fe_{HR}/Fe_T) of the shale interbeds were almost all >0.38, consistent with values associated with modern marine sediments deposited under anoxic water column conditions (Fig. 6a). Only four samples, all in the *N. kozlowskii* zone, fell within the 0.22–0.38 range, representing possibly anoxic or fluctuating redox conditions in the water column (Poulton and Canfield 2005;

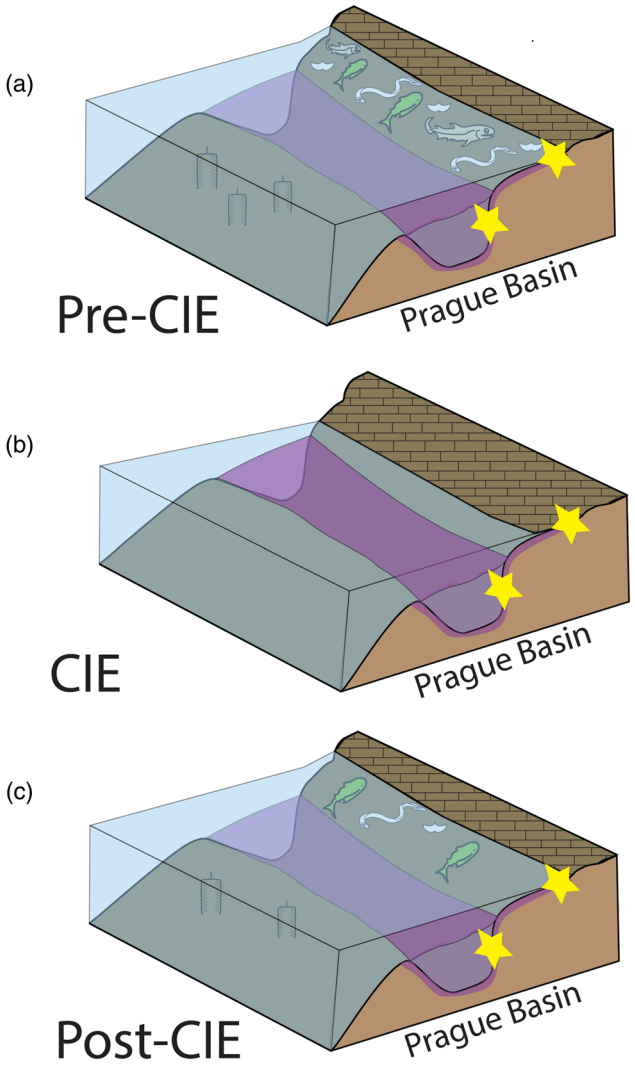

Fig. 9. Schematic drawing of the extent of anoxia through time along an idealized transect of the semi-restricted Prague Basin based on proxy data. Approximate locations of the Mušlovka and Kosov Quarry sections are marked by stars. Reducing conditions in both the water column and sediment porewaters are represented by transparent purple overlay. See text for discussion and compare with the model in Frýda *et al.* (2021*b*, their fig. 9). CIE, C isotope excursion.

Raiswell *et al.* 2018). The pyrite to highly reactive Fe (Fe_{pyr}/Fe_{HR}) values plot almost entirely within the ferruginous field (<0.7), with only four samples plotting as possibly euxinic to euxinic within the LKE interval (Fig. 6b). These new Fe speciation data suggest that the local bottom waters were reducing before, during and after this global marine extinction event (Fig. 9), but sulfide was likely limited with relatively little formation of pyrite from reactive Fe minerals.

These trends are consistent with previously published Fe speciation data from the Priekule-20 drill core deposited in the deep shelf of the Baltic Basin, which show a local pulse of sulfidic sediment porewater conditions during roughly the same stratigraphic interval during the LKE event (Bowman *et al.* 2021). Similarly, samples from the Richardson Trough in the Yukon of NW Canada indicate that anoxic areas of the late Silurian ocean were ferruginous, but likely not euxinic, through the LKE and Lau CIE on the northern margin of Laurentia (Sperling *et al.* 2021).

The Fe_T/Al ratios were somewhat variable through the Kosov Quarry section, between 0.47 and 0.87 (Fig. 6c). These values were compared with the average value for Paleozoic oxic marine shales of 0.53 ± 0.11 (Raiswell *et al.* 2018). Fe_T/Al values >0.64 are typically indicative of benthic Fe shuttling within a basin (e.g. Raiswell *et al.* 2018). The Fe_T/Al ratios average 0.64, with most values above the Paleozoic average, indicating the likelihood of some benthic Fe shuttling from shallow to deep shelf sediments in the Prague Basin during the Ludfordian. These values could suggest a variation in the locus of reducing conditions throughout the Ludfordian in the deep shelf of the Prague Basin, with the Fe reduction zone moving back and forth across the sediment–water interface (Fig. 9; Hardisty *et al.* 2018; Raiswell *et al.* 2018).

The reported trace metal concentrations discussed in the following have been corrected for variable lithological changes, such as carbonate content, and then for all trace metals aside from Mn, normalized with the TOC content from each sample. The Mn concentrations recorded from the Kosov Quarry section average *c.* 175 ppm throughout the section with no notable trend, well below the average of 850 ppm for modern oxic sediments (Fig. 6d; Morford and Emerson 1999). There are a few data points with relatively high values in the *P. dubius postfrequens* and *M. latilobus–S. balticus* graptolite zones, but even these are still well below the modern oxic sediment average. These [Mn] data are indicative of bottom waters that were suboxic to anoxic, preventing the long-term burial of Mn oxides. This is consistent with the independent findings of the Fe speciation proxy suggesting consistent locally anoxic water column conditions (Fig. 9).

V requires local suboxic to anoxic water column conditions to become enriched within sediments, but not necessarily euxinic conditions (Algeo and Maynard 2004; Owens *et al.* 2016, 2017). TOC-normalized V concentrations in the Kosov Quarry are moderately enriched in the *N. inexpectatus* and *N. kozlowskii* zones, averaging *c.* 340 ppm/wt%, and decrease through the LKE interval to *c.* 157 ppm/wt% (Fig. 6e). The moderate V/TOC enrichments throughout the section are consistent with locally suboxic–anoxic water columns. Trends between the carbonate-corrected and TOC-normalized [V] are similar, highlighting the possibility of a shift in the global V reservoir rather than the local influence of variable organic matter deposition in the Prague Basin (Algeo and Rowe 2012). The trend in V/TOC from higher to lower values moving upwards throughout the section could indicate a trend from anoxic to more suboxic or fluctuating redox conditions, although there was no corresponding change in Fe speciation data to support this. Alternatively, this trend towards lower [V] might be reflective of changes in the global inventory of V in the late Silurian oceans.

The TOC-normalized U concentrations range from *c.* 10 to 150 ppm/wt% in the Kosov Quarry section (Fig. 6f). The accumulation of U in sediments is reliant on the diffusion of uranyl carbonate ions and the reduction from U^{6+} to U^{4+} across the sediment–water interface. Enriched U concentrations therefore indicate anoxic bottom water conditions (Tribovillard *et al.* 2006). Across the upper boundary of the *N. kozlowskii* biozone, the average U/TOC ratio decreases slightly from 73 to 66 ppm/wt%. Overall, the U/TOC data suggest relatively consistent bottom water anoxia through the Ludfordian, in agreement with the Fe speciation and [Mn] data (Fig. 9).

Mild enrichments in Mo were also preserved in the Kosov Quarry section. Mo requires euxinic conditions to significantly enrich in sediments and is often associated with the burial of organic carbon (Fig. 6g). The Mo/TOC ratio averaged *c.* 23 ppm/wt% and, taken together with the Fe speciation data, suggests predominantly anoxic water column conditions with possibly sulfidic sediment porewaters (Fig. 9; Hardisty *et al.* 2018). As with V and U, there was a notable decrease in Mo/TOC across the upper boundary of the *N. kozlowskii* zone from an average of *c.* 27 to *c.* 20 ppm/wt%. The Mo/TOC values at Kosov Quarry are similar to those of the modern day silled Cariaco Basin (Fig. 9; Algeo and Lyons 2006) and could suggest some minor amount of hydrographic restriction for the Prague Basin, as suggested by Frýda *et al.* (2021*b*), but certainly point to a continued connection with the open ocean to allow for such elevated enrichments.

The trends in the TOC-normalized concentrations of V, U and Mo from the shale interbeds of Kosov Quarry in this study correspond well to those published by Frýda *et al.* (2021*b*) from both the shale and carbonate interbeds (compare their fig. 6 with Fig. 6e–g of this study) and similar data in the same time interval from the deep shelf of the Baltic Basin published by Bowman *et al.* (2021). The decreases in redox-sensitive trace element concentrations during the Lau CIE and after the LKE event are even more notable in the data from Frýda *et al.* (2021*b*) because they have a higher sampling density from the inclusion of the limestone and marl interbeds in the geochemical analyses.

Based on the calculated values for U and Mo enrichment factors, both trace elements show substantial enrichment throughout the shales of Kosov Quarry, with almost all U_{EF} and Mo_{EF} values >10 (Algeo and Tribovillard 2009). This further supports the view that local marine redox conditions were reducing throughout the Ludfordian (Fig. 9). The generally higher U_{EF} values than Mo_{EF} values, averages of 22 and 16, respectively, imply that suboxic to anoxic conditions were dominant as opposed to euxinic conditions. This indicates that the Fe reduction zone was likely at or near the sediment–water interface, allowing for the additional enrichment of U and bolstering the interpretations of local redox conditions from the Fe speciation data (Morford and Emerson 1999; Algeo and Tribovillard 2009).

Cross-plots of U_{EF} and Mo_{EF} can also be used to interpret basin connectivity based on the comparison of Mo/U molar ratios with those of open ocean seawater (*c.* 7.5–7.9; Algeo and Tribovillard 2009). These ratios are shown as parallel lines on U_{EF} and Mo_{EF} cross-plots (Fig. 7). The Mo/U ratios for the Kosov Quarry shale interbeds fall primarily between 0.1 and 0.3 times the molar ratio of seawater, indicating that the samples were likely deposited either under fluctuating redox conditions or in a restricted basin (Fig. 7, blue symbols; Algeo and Tribovillard 2009). The presence of cosmopolitan conodont and graptolite fauna throughout both the Mušlovka and Kosov Quarry sections requires a strong connection to the open ocean and prohibits the possibility of complete restriction (Havlíček and Štorch 1990; Kříž 1991; 1992; Manda 2008). This provides further evidence that the Kosov Quarry shales were deposited in a silled marine basin, as previously suggested, due to active Silurian faulting and volcanic activity in the region (e.g. Tasáryová *et al.* 2018). Slight hydrographic restriction due to a marine sill in the Prague Basin may help to explain the coincidence of low Mo/U values with the cosmopolitan marine fauna (Fig. 9).

Frýda *et al.* (2021*b*) also published Mo/U molar ratios from Kosov Quarry. Their U_{EF} and Mo_{EF} data, which include samples from the limestone and marl interbeds, has a much wider spread, ranging from 0.1 to 1.0 times the molar ratio of seawater (Fig. 7,

pink and green symbols). The larger range in their U_{EF} and Mo_{EF} data could reflect variations in the specific part of the shelf the sediments were formed in, with sediments initially recording the local marine redox conditions in those (shallower) locations and then subsequently transported to this deep shelf setting. Specifically, this deep shelf setting consists of alternating beds of shale and carbonate lithologies, with the carbonates interpreted to be tempestites (i.e. storm deposits from the nearby shallow carbonate bank), not formed *in situ*, but transported some distance (Manda *et al.* 2012; Gocke *et al.* 2013). Consequently, the interbeds of shale–mudstone should record the 'background' sedimentation and therefore local marine redox conditions more representative of the Kosov Quarry deep shelf environment. The overall higher degree of variability in the U_{EF} and Mo_{EF} data of Frýda *et al.* (2021*a*) may therefore reflect the variation in strata that is representative of background sedimentation at Kosov Quarry as well as being reflective of other shallower marine environments nearby (e.g. the use of both carbonates and mudstone/shales).

Alternatively, their data may track the evolution of water mass chemistry due to the interplay of global and local sea-level change within the Prague Basin. During the Ludfordian, the sea-level has been inferred from sequence stratigraphic models to be the lowest during the Lau CIE, during the mid-Ludfordian glaciation, with relatively high sea-levels pre- and post-CIE (e.g. Lehnert *et al.* 2007; Eriksson and Calner 2008; Frýda *et al.* 2021*b*). There were overall higher authigenic enrichments of redox-sensitive trace metals prior to the Lau CIE (Fig. 7, pink symbols; Frýda *et al.* 2021*a*), during times of globally higher sea-level, suggesting that the Prague Basin was well connected to the Rheic Ocean. For some of the Frýda *et al.* (2021*a*) pre-excursion data, $Mo_{EF} > U_{EF}$ (higher Mo/U), which may be related to the enrichment of Mo in sulfidic porewaters within nearby shallow carbonate sediments washed in as tempestite beds (Fig. 9).

During the Lau CIE (interval II, see Frýda *et al.* 2021*a*, *b*), authigenic enrichments were lower within the carbonate interbeds at a time when the global sea-level was at its lowest (Fig. 9b). Low authigenic enrichments and low Mo/U ratios during this global sea-level low are analogous to the record of enrichments and Mo/U ratios along the basin margins of the Black Sea (Algeo and Tribovillard 2009). This implies the sediments of the carbonate tempestite beds may have formed under an oxic water column in the mixed zone of the shallow shelf before being transported and deposited at the relatively deeper Kosov Quarry location. When combined with the relatively consistent Mo/U ratios (*c.* 0.2–0.3) and high authigenic enrichment data from the shale interbeds, these data are even more comparable to those of the Black Sea and may further suggest that the Prague Basin was silled (Fig. 9).

The bulk of the $\delta^{34}S_{pyr}$ data documented at the Kosov Quarry most likely reflect global changes in pyrite burial and euxinia and are discussed later; here, we discuss trends and excursions in the $\delta^{34}S_{pyr}$ data that are more likely related to local factors. The large degree of scatter in the $\delta^{34}S_{pyr}$ data in the lower part of the section within the *N. inexpectatus* zone is likely a result of changes in local factors affecting MSR, such as the location of pyrite formation – in either the water column or sediment porewaters – or variations in the availability of sulfate for MSR and/or reactive Fe for the formation of pyrite. Post-CIE, in the *M. latilobus–S. balticus* and *M. fragmentalis* zones, there is an apparent second positive excursion in $\delta^{34}S_{pyr}$ of >30‰. Frýda *et al.* (2021*a*) interpret this as a continuation of the main $\delta^{34}S_{pyr}$ excursion that was interrupted with a negative isotope excursion in the lower–middle *M. latilobus–S. balticus* zone, which resulted from an influx of isotopically negative sulfate from the open ocean during a transgression to temporarily fuel the production of hydrogen sulfide via MSR.

Frýda *et al.* (2021*b*) noted that occurrence of new faunal communities at this stratigraphic level supports a hypothesis of a temporary influx of better oxygenated ocean waters into a partly restricted epeiric basin as a driver for the rapid decrease in the $\delta^{34}S_{pyr}$ signal. However, there is no corresponding increase in pyrite concentrations documented at Kosov Quarry at that time (Frýda *et al.* 2021*b*). The delayed return to baseline values of $\delta^{34}S$ relative to $\delta^{13}C$ in the Lau CIE has been recorded in several other Ludfordian sections from Laurentia and Baltica (Bowman *et al.* 2020, 2021), although it is not clear if this is the cause of the apparently additional $\delta^{34}S_{pyr}$ excursion seen here. The offset between these two stable isotope records may be linked to a continuation of enhanced pyrite burial rates due to the accumulation of labile organic matter (i.e. Lau CIE-related C_{org} burial) on the seafloor and within the upper parts of the marine sediments.

Implications for Ludfordian global redox changes

The parallel $\delta^{13}C_{carb}$ and $\delta^{34}S_{pyr}$ excursions recorded from this locally anoxic marine setting in the Prague Basin (Frýda *et al.* 2021*b* and this study), when combined with stable isotopic records from other palaeocontinents (e.g. $\delta^{34}S_{CAS}$), suggest that major changes in global marine redox conditions occurred during this interval of the late Silurian. These positive C and S isotopic excursions imply the enhanced burial of reduced C and S as organic matter, pyrite and organic S compounds (Gill *et al.* 2011*a*; Owens *et al.* 2013). The high magnitude S isotope excursion recorded both in sedimentary pyrite from our shale interbed samples (+30‰ in $\delta^{34}S_{pyr}$; Fig. 5b, red symbols) and the sedimentary pyrite from marl and limestone samples (+20‰ in $\delta^{34}S_{pyr}$; Fig. 5b, blue symbols) recently published by Frýda *et al.* 2021(*a*, *b*) from the Kosov Quarry section correlate with the +20 to +68‰ magnitude $\delta^{34}S_{pyr}$ excursions documented in Baltica (Bowman *et al.* 2019, 2021) and in southern Laurentia (Bowman *et al.* 2020) during the LKE and Lau CIE interval.

The positive excursion in $\delta^{34}S_{CAS}$ records from shallow shelf carbonates of the Baltic Basin (+30‰), the southern margin of Laurentia (+8‰) and deeper shelf of the peri-Gondwana (+15‰) indicate that there was not only an expansion of anoxia in the mid-Ludfordian (Fig. 9), but also enhanced pyrite burial on many continental margin settings at this time due to expanded euxinic bottom water conditions (Bowman *et al.* 2019, 2020; Frýda *et al.* 2021*a*, *b*). A recent study of $\delta^{238}U$ records (del Rey *et al.* 2023) from temperate (Kosov, peri-Gondwana) and tropical (Broken River, eastern Gondwana) settings also support previous findings (Bowman *et al.* 2019; Frýda *et al.* 2021*b*) that reducing conditions expanded in the global oceans before and during the onset of the Lau CIE and were contemporaneous with the faunal extinctions during the LKE event.

The onset of the positive excursion in $\delta^{34}S_{pyr}$ from Kosov Quarry occurs stratigraphically higher (after) the onset of the Lau CIE in both our dataset and the Frýda *et al.* (2021*a*) dataset. This offset pattern in $\delta^{34}S$ relative to $\delta^{13}C$ at Kosov Quarry is consistent with previously published paired C and S records from other palaeo-continents and supports the hypothesis that, in the mid-Ludfordian, enhanced organic C burial predated increased pyrite burial and the expansion of euxinic conditions (Bowman *et al.* 2020; 2021; Frýda *et al.* 2021*b*).

Although the trends in trace elements in the Kosov Quarry have been interpreted here to represent changes in the local redox conditions, inferences can be drawn about global redox changes when these data are considered within the context of time-correlative local and global marine redox proxy data from other palaeo-ocean basins (i.e. Bowman *et al.* 2019, 2020, 2021; Frýda *et al.* 2021*a*, *b*). In the Kosov Quarry section, trace metal concentrations decrease from the *N. kozlowskii* through the *P. dubius postfrequens* zones, coincident with the positive excursion of $\delta^{34}S_{pyr}$ and $\delta^{34}S_{CAS}$ that is linked to the expansion of euxinic conditions globally. Reducing sediments more readily

sequester trace metals as anoxic to euxinic conditions expand along continental margins throughout global oceans (Owens *et al.* 2016). A decrease in trace metal concentrations (V, Hg, U and Mo) during this same approximate time interval is also recorded in the Priekule-20 core from Latvia (Baltic Basin; Bowman *et al.* 2021) and trace metal datasets previously reported from marl and limestone interbeds from Kosov Quarry (Frýda *et al.* 2021*b*). Collectively, these data suggest that bottom water deoxygenation may have led to global trace metal drawdown during the Lau CIE (e.g. Owens *et al.* 2016; Frýda *et al.* 2021*b*). Ultimately, additional Ludfordian trace metal records from globally dispersed localities are needed from shale successions that were persistently euxinic throughout this time interval to definitively test this hypothesis.

Conclusions

We have presented new geochemical redox proxy data from the shallow shelf carbonates of the Mušlovka Quarry section and the shale interbeds from the deeper shelf section at Kosov Quarry, both from the Prague Basin of the mid-latitude peri-Gondwanan Barrandian Terrane. Initial microfacies analysis of the Mušlovka Quarry section show that diagenetic processes notably affected primary carbonate textures through dolomitization, recrystallization, and common secondary calcite veins and euhedral pyrite. There is no significant stratigraphic trend in the I/Ca and $\delta^{34}S_{pyr}$ records from Mušlovka Quarry. The low I/Ca values throughout the Mušlovka Quarry section could be reflective of either consistent local anoxic waters nearby or diagenetic overprinting during the complex tectonic and burial history of this region. However, elevated pyrite concentrations indicate that the local marine environment was most likely reducing in the sediment porewaters at the very least. The $\delta^{34}S_{pyr}$ values at Mušlovka Quarry appear to reflect local sulfur cycling within the likely sulfidic sediment porewaters. The high pyrite contents of the Mušlovka Quarry carbonates suggest that the majority of our $\delta^{34}S_{CAS}$ data presented here are consistent with contamination via pyrite oxidation during the chemical extraction process for CAS.

In the Kosov Quarry, Fe speciation data suggest a locally anoxic marine water column throughout the sampled succession, with intervals of benthic Fe shuttling. Consistently low concentrations of Mn support the interpretation of water column anoxia, particularly bottom water anoxia, which would have prevented the accumulation of Mn oxides. Enrichments in redox-sensitive trace elements throughout the section are also consistent with local anoxia. The excursion in $\delta^{34}S_{pyr}$ values from Kosov Quarry coincident with the Lau CIE suggests increased reduced carbon and sulfur burial as organic matter and pyrite (Gill *et al.* 2011*a*; Owens *et al.* 2013). The trends in the $\delta^{34}S_{pyr}$ data from Kosov Quarry likely reflect the global enhancement of pyrite burial and euxinia in the Ludfordian oceans. Notable drawdowns in redox-sensitive trace elements (V, U and Mo) in the same stratigraphic interval from two hydrographically separated and geographically disparate ocean basins further support the severity and global nature of the marine redox changes associated with the LKE (Laurentia, Tennessee Shelf, Bowman *et al.* 2020; Baltic Basin, Bowman *et al.* 2021; Prague Basin, this study; Frýda *et al.* 2021*b*). However, more work is needed from Ludfordian sections with evidence of persistent local euxinia to better test this trace metal drawdown hypothesis.

This multiproxy, multi-lithology investigation gives a holistic perspective on local and global redox changes in the late Silurian oceans. Expanded marine anoxia and/or euxinia provides a plausible mechanism for the LKE because deoxygenated waters containing appreciable free hydrogen sulfide would have induced significant stress on marine life (e.g. Meyer and Kump 2008). The extent and severity of the expansive reducing conditions during the Lau CIE and LKE has become much clearer, despite the complications and complexities inherent to unravelling ancient local and global marine redox conditions.

Scientific editing by Simon Poulton

Acknowledgements We thank Sean Newby for assistance in sample processing and data collection. We thank two anonymous reviewers and Editor Simon Poulton for their detailed and constructive feedback, which helped to improve this paper.

Author contributions **LJA**: conceptualization (supporting), data curation (equal), formal analysis (equal), investigation (equal), writing – original draft (lead); **CNB**: conceptualization (equal), data curation (equal), formal analysis (equal), investigation (equal), writing – original draft (equal); **JF**: conceptualization (supporting), funding acquisition (supporting), investigation (supporting), writing – review and editing (equal); **NPK**: formal analysis (supporting), investigation (equal), writing – review and editing (equal); **JDO**: conceptualization (supporting), formal analysis (supporting), funding acquisition (equal), supervision (supporting), writing – review and editing (equal); **SAY**: conceptualization (equal), funding acquisition (equal), investigation (equal), supervision (lead), writing – review and editing (equal).

Funding This research was funded by the National Science Foundation (EAR-1748635 to SAY and JDO) and by the Grant Agency of the Czech Republic (GA23-06198S to JF). This research was performed at the National High Magnetic Field Laboratory, which is supported by NSF Cooperative Agreement No. DMR-1644770 and the State of Florida.

Competing interests The authors declare that they have no known competing financial interests or personal relationships that could have appeared to influence the work reported in this paper.

Data availability The datasets used for this article are available in the Supplementary material.

References

Algeo, T.J. and Lyons, T.W. 2006. Mo-total organic carbon covariation in modern anoxic marine environments: implications for analysis of paleoredox and paleohydrographic conditions. *Paleoceanography*, **21**, PA1016, https://doi.org/10.1029/2004PA001112

Algeo, T.J. and Maynard, J.B. 2004. Trace-element behavior and redox facies in core shales of Upper Pennsylvanian Kansas-type cyclothems. *Chemical Geology*, **206**, 289–318, https://doi.org/10.1016/j.chemgeo.2003.12.009

Algeo, T.J. and Rowe, H. 2012. Paleoceanographic applications of trace-metal concentration data. *Chemical Geology*, **324–325**, 6–18, https://doi.org/10.1016/j.chemgeo.2011.09.002

Algeo, T.J. and Tribovillard, N. 2009. Environmental analysis of paleoceanographic systems based on molybdenum–uranium covariation. *Chemical Geology*, **268**, 211–225, https://doi.org/10.1016/j.chemgeo.2009.09.001

Banner, J.L. and Hanson, G.N. 1990. Calculation of simultaneous isotopic and trace element variations during water–rock interaction with applications to carbonate diagenesis. *Geochimica et Cosmochimica Acta*, **54**, 3123–3137, https://doi.org/10.1016/0016-7037(90)90128-8

Bickert, T., Patzold, J., Samtleben, C. and Munnecke, A. 1997. Paleoenvironmental changes in the Silurian indicated by stable isotopes in brachiopod shells from Gotland, Sweden. *Geochimica et Cosmochimica Acta*, **61**, 2717–2730, https://doi.org/10.1016/S0016-7037(97)00136-1

Bond, D.P.G. and Grasby, S.E. 2017. On the causes of mass extinctions. *Palaeogeography, Palaeoclimatology, Palaeoecology*, **478**, 3–29, https://doi.org/10.1016/j.palaeo.2016.11.005

Bowman, C.N., Young, S.A. *et al.* 2019. Linking the progressive expansion of reducing conditions to a stepwise mass extinction event in the late Silurian oceans. *Geology*, **47**, 968–972, https://doi.org/10.1130/G46571.1

Bowman, C.N., Lindskog, A., Kozik, N.P., Richbourg, C.G., Owens, J.D. and Young, S.A. 2020. Integrated sedimentary, biotic, and paleoredox dynamics from multiple localities in southern Laurentia during the late Silurian (Ludfordian) extinction event. *Palaeogeography, Palaeoclimatology, Palaeoecology*, **553**, 109799, https://doi.org/10.1016/j.palaeo.2020.109799

Bowman, C.N., Them, T.R.,II, *et al.* 2021. A multi-proxy approach to constrain reducing conditions in the Baltic Basin during the late Silurian Lau carbon isotope excursion. *Palaeogeography, Palaeoclimatology, Palaeoecology*, **581**, 110624, https://doi.org/10.1016/j.palaeo.2021.110624

Brüchert, V. and Pratt, L.M. 1996. Contemporaneous early diagenetic formation of organic and inorganic sulfur in estuarine sediments from St. Andrew Bay, Florida, USA. *Geochimica et Cosmochimica Acta*, **60**, 2325–2332, https://doi.org/10.1016/0016-7037(96)00087-7

Calner, M. 2008. Silurian global events – at the tipping point of climate change. *In*: Elewa, A.M.T. (eds) *Mass Extinctions*. Springer, Berlin, 21–58, https://doi.org/10.1007/978-3-540-75916-4_4

Canfield, D.E. and Thamdrup, B. 1994. The production of ^{34}S-depleted sulfide during bacterial disproportionation of elemental sulfur. *Science*, **266**, 1973–1975, https://doi.org/10.1126/science.11540246

Canfield, D.E., Raiswell, R., Westrich, J.T., Reaves, C.M. and Berner, R.A. 1986. The use of chromium reduction in the analysis of reduced inorganic sulfur in sediments and shales. *Chemical Geology*, **54**, 149–155, https://doi.org/10.1016/0009-2541(86)90078-1

Chadimova, L., Vacek, F., Sobien, K., Slavik, L. and Hladil, J. 2015. Petrophysical record of the Late Silurian shallow-water carbonate facies across the Lau Event (Prague Synform, Czech Republic) and dynamic time warping alignment of the magnetic susceptibility logs. *Geological Society, London, Special Publications*, **414**, 133–155, https://doi.org/10.1144/SP414.14

Cocks, L.R.M. and Torsvik, T.H. 2002. Earth geography from 500 to 400 million years ago: a faunal and paleomagnetic review. *Journal of the Geological Society, London*, **159**, 631–644, https://doi.org/10.1144/0016-764901-118

Cramer, B.D. and Saltzman, M.R. 2005. Sequestration of ^{12}C in the deep ocean during the early Wenlock (Silurian) positive carbon isotope excursion. *Palaeogeography, Palaeoclimatology, Palaeoecology*, **219**, 333–349, https://doi.org/10.1016/j.palaeo.2005.01.009

Cramer, B.D. and Saltzman, M.R. 2007. Fluctuations in epeiric sea carbonate production during Silurian positive carbon isotope excursions: a review of proposed paleoceanographic models. *Palaeogeography, Palaeoclimatology, Palaeoecology*, **245**, 37–45, https://doi.org/10.1016/j.palaeo.2006.02.027

Crampton, J.S., Cooper, R.A., Sadler, P.M. and Foote, M. 2016. Greenhouse–icehouse transition in the Late Ordovician marks a step change in extinction regime in the marine plankton. *Proceedings of the National Academy of Sciences of the USA*, **113**, 1498–1503, https://doi.org/10.1073/pnas.1519092113

del Rey, A., Havsteen, J.C., Bizarro, M. and Dahl, T.W. 2020. Untangling the diagenetic history of uranium isotopes in marine carbonates: a case study tracing the δ^{238}U composition of late Silurian oceans using calcitic brachiopod shells. *Geochimica et Cosmochimica Acta*, **287**, 93–110, https://doi.org/10.1016/j.gca.2020.06.002

del Rey, Á., Frýda, J. *et al.* 2023. Mid-Ludfordian uranium isotope records distinguish the role of expansive marine anoxia in global carbon cycle dynamics during the late Silurian Lau/Kozlowskii bioevent. *Planetary and Global Change*, **229**, 104248, https://doi.org/10.1016/j.gloplacha.2023.104248

Edwards, C.T., Fike, D.A. and Saltzman, M.R. 2019. Testing carbonate-associated sulfate (CAS) extraction methods for sulfur isotope stratigraphy: a case study of a Lower–Middle Ordovician carbonate succession, Shingle Pass, Nevada, USA. *Chemical Geology*, **529**, 119297, https://doi.org/10.1016/j.chemgeo.2019.119297

Epstein, A.G., Epstein, J.B. and Harris, L.D. 1977. Conodont color alteration – an index to organic metamorphism. *United States Geological Survey, Professional Papers*, **995**, 1–27, https://doi.org/10.3133/pp995

Eriksson, M.J. and Calner, M. 2008. A sequence stratigraphical model for the late Ludfordian (Silurian) of Gotland, Sweden: implications for timing between changes in sea level, palaeoecology, and global carbon cycle. *Facies*, **54**, 253–276, https://doi.org/10.1007/s10347-007-0128-y

Eriksson, M.E., Nilsson, E.K. and Jeppsson, L. 2009. Vertebrate extinctions and reorganizations during the Late Silurian Lau Event. *Geology*, **37**, 739–742, https://doi.org/10.1130/G25709A.1

Farkaš, J., Frýda, J. and Holmden, C. 2016. Calcium isotope constraints on the marine carbon cycle and $CaCO_3$ deposition during the late Silurian positive δ^{13}C excursion. *Earth and Planetary Science Letters*, **451**, 31–40, https://doi.org/10.1016/j.epsl.2016.06.038

Ferretti, A. and Kříž, J. 1995. Cephalopod limestone biofacies in the Silurian of the Prague Basin, Bohemia. *Palaios*, **10**, 240–253, https://doi.org/10.2307/3515255

Frýda, J. and Manda, Š. 2013. A long-lasting steady period of isotopically heavy carbon in the late Silurian ocean: evolution of the δ^{13}C record and its significance for an integrated δ^{13}C, graptolite and conodont stratigraphy. *Bulletin of Geosciences*, **88**, 463–482, https://doi.org/10.3140/bull.geosci.1436

Frýda, J., Lehnert, O., Frýdová, B., Farkaš, J. and Kubajko, M. 2021*a*. Carbon and sulfur cycling during the mid-Ludfordian anomaly and the linkage with the late Silurian Lau/Kozlowskii Bioevent. *Palaeogeography, Palaeoclimatology, Palaeoecology*, **564**, 110152, https://doi.org/10.1016/j.palaeo.2020.110152

Frýda, J., Lehnert, O. *et al.* 2021*b*. The Mid-Ludfordian (late Silurian) glaciation: a link with global changes in ocean chemistry and ecosystem overturns. *Earth-Science Reviews*, **220**, 103652, https://doi.org/10.1016/j.earscirev.2021.103652

Gill, B.C., Lyons, T.W. and Frank, T.D. 2008. Behavior of carbonate-associated sulfate during meteoric diagenesis and implications for the sulfur isotope paleoproxy. *Geochimica et Cosmochimica Acta*, **72**, 4699–4711, https://doi.org/10.1016/j.gca.2008.07.001

Gill, B.C., Lyons, T.W. and Jenkyns, H.C. 2011*a*. A global perturbation to the sulfur cycle during the Toarcian oceanic anoxic event. *Earth and Planetary Science Letters*, **312**, 484–496, https://doi.org/10.1016/j.epsl.2011.10.030

Gill, B.C., Lyons, T.W., Young, S.A., Kump, L.R., Knoll, A.H. and Saltzman, M.R. 2011*b*. Geochemical evidence for widespread euxinia in the later Cambrian ocean. *Nature*, **469**, 80–83, https://doi.org/10.1038/nature09700

Gocke, M., Lehnert, O. and Frýda, J. 2013. Facies development and palynomorphs during the Lau Event (Late Silurian) in a non-tropical carbonate environment: shallow and deep water examples from the Barrandian Area (Czech Republic). *Facies*, **59**, 611–630, https://doi.org/10.1007/s10347-012-0328-y

Gomes, M.L. and Hurtgen, M.T. 2015. Sulfur isotope fractionation in modern euxinic systems: implications for paleoenvironmental reconstructions of paired sulfate–sulfide isotope records. *Geochimca et Cosmochimica Acta*, **157**, 39–55, https://doi.org/10.1016/j.gca.2015.02.031

Hackley, P.C. and Cardott, B.J. 2016. Application of organic petrography in North American shale petroleum systems: a review. *International Journal of Coal Geology*, **163**, 8–51, https://doi.org/10.1016/j.coal.2016.06.010

Hardisty, D.S., Lu, Z., Planavsky, N.J., Bekker, A., Philippot, P., Zhou, X. and Lyons, T.W. 2014. An iodine record of Paleoproterozoic surface ocean oxygenation. *Geology*, **42**, 619–622, https://doi.org/10.1130/G35439.1

Hardisty, D.S., Lu, Z. *et al.* 2017. Perspectives on Proterozoic surface ocean redox from iodine contents in ancient and recent carbonate. *Earth and Planetary Science Letters*, **463**, 159–170, https://doi.org/10.1016/j.epsl.2017.01.032

Hardisty, D.S., Lyons, T.W. *et al.* 2018. An evaluation of sedimentary molybdenum and iron as proxies for pore fluid paleoredox conditions. *American Journal of Science*, **318**, 527–556, https://doi.org/10.2475/05.2018.04

Havlíček, V. and Štorch, P. 1990. Silurian brachiopods and benthic communities in the Prague Basin (Czechoslovakia). *Rozpravy Ústředního ústavu geologického*, **48**, 1–275.

Havlíček, V., Vaněk, J. and Fatka, O. 1994. Perunica microcontinent in the Ordovician (its position within the Mediterranean Province, series division, benthic and pelagic associations). *Sborník geologických věd, Paleontologie*, **46**, 23–56.

Hrubcová, P., Środa, P., Grad, M., Geissler, W.H., Guterch, A., Vozár, J., Hegedus, E. and Sudetes 2003 Working Group 2010. From the Variscan to the Alpine Orogeny: crustal structure of the Bohemian Massif and the Western Carpathians in the light of the SUDETES 2003 seismic data. *Geophysical Journal International*, **183**, 611–633, https://doi.org/10.1111/j.1365-246X.2010.04766.x

Hurtgen, M.T., Arthur, M.A., Suits, N.S. and Kaufman, A.J. 2002. The sulfur isotopic composition of Neoproterozoic seawater sulfate: implications for a snowball Earth? *Earth and Planetary Science Letters*, **203**, 413–429, https://doi.org/10.1016/S0012-821X(02)00804-X

Jeppsson, L. 1990. An oceanic model for lithological and faunal changes tested on the Silurian record. *Journal of the Geological Society, London*, **147**, 663–674, https://doi.org/10.1144/gsjgs.147.4.0663

Jeppsson, L. 2005. Conodont-based revisions of the Late Ludfordian on Gotland, Sweden. *Geologiska Föreningens i Stockholm Förhandlingar*, **127**, 273–282, https://doi.org/10.1080/11035890501274273

Jeppsson, L. and Aldridge, R.J. 2000. Ludlow (late Silurian) oceanic episodes and events. *Journal of the Geological Society, London*, **157**, 1137–1148, https://doi.org/10.1144/jgs.157.6.1137

Jeppsson, L. and Landing, E. 1998. Silurian oceanic events: summary of general characteristics. *New York State Museum Bulletin*, **491**, 239–257.

Jones, D.S. and Fike, D.A. 2013. Dynamic sulfur and carbon cycling through the end-Ordovician extinction revealed by paired sulfate–pyrite δ^{34}S. *Earth and Planetary Science Letters*, **363**, 144–155, https://doi.org/10.1016/j.epsl.2012.12.015

Kaljo, D., Kiipli, T. and Martma, T. 1997. Carbon isotope event markers through the Wenlock–Pridoli sequence at Ohesaare (Estonia) and Priekule (Latvia). *Palaeogeography, Palaeoclimatology, Palaeoecology*, **132**, 211–223, https://doi.org/10.1016/S0031-0182(97)00065-5

Koren', T.N. 1993. Main event levels in the evolution of the Ludlow graptolites. *Geological Magazine*, **1**, 44–52, https://doi.org/10.1017/S0016756811000847

Kozik, N.P., Gill, B.C., Owens, J.D., Lyons, T.W. and Young, S.A. 2022. Geochemical records reveal protracted and differential marine redox change associated with late Ordovician climate and mass extinctions. *AGU Advances*, **3**, 1, https://doi.org/10.1029/2021AV000563

Kozłowski, W. 2015. Eolian dust influx and massive whitings during the Kozlowski/Lau Event: carbonate hypersaturation as a possible driver of the mid-Ludfordian carbon isotope excursion. *Bulletin of Geosciences, Czech Geological Survey*, **90**, 807–840, https://doi.org/10.3140/bull.geosci.1581

Kříž, J. 1991. The Silurian of the Prague Basin (Bohemia): tectonic, eustatic, and volcanic controls on facies and faunal development. *Special Papers in Palaeontology*, **44**, 179–204.

Kříž, J. 1992. *Silurian Field Excursions: Prague Basin (Barrandian), Bohemia*. National Museum of Wales, Cardiff, Geological Series, **13**.

Kříž, J. 1999. Bivalvia dominated communities of Bohemian type from the Silurian and Lower Devonian carbonate facies. *In*: Boucot, A.J. and Lawson, J.D. (eds) *Final Report, Project Ecostratigraphy. Paleocommunities: A Case Study from the Silurian and Lower Devonian*. Cambridge University Press, 225–248, https://doi.org/10.1016/S0016-6995(95)80062-X

Kříž, J. 2008. *Algerina* gen. nov. (Bivalvia, Nepiomorphia) from the Silurian of the North Gondwana margin (Algeria), peri-Gondwanan Europe (France, Italy), Perunica (Prague Basin, Bohemia) and the Siberian Plate (Tajmyr Basin, Russia). *Bulletin of Geosciences, Czech Geological Survey*, **83**, 79–84, https://doi.org/10.3140/bull.geosci.2008.01.079

Kříž, J. and Schönlaub, H.P. 1980. Stop 1. Daleje Valley, Mušlovka Quarry section. *Abhanlungen der Geologischen Bundesanstalt*, **35**, 147–180.

Lau, K.V. and Hardisty, D.S. 2022. Modeling the impacts of diagenesis on carbonate paleoredox proxies. *Geochimica et Cosmochimica Acta*, **337**, 123–139, https://doi.org/10.1016/j.gca.2022.09.021

Leavitt, W.D., Halevy, I., Bradley, A.S. and Johnston, D.T. 2013. Influence of sulfate reduction rates on the Phanerozoic sulfur isotope record. *Proceedings of the National Academy of Sciences, USA*, **110**, 11244–11249, https://doi.org/10.1073/pnas.1218874110

Lehnert, O., Frýda, J., Buggisch, W. and Manda, S. 2003. A first report of the Ludlovian Lau event from the Prague Basin (Barrandian, Czech Republic). *In*: Ortega, G. and Aceñolaza, G.F. (eds) Proceedings of the 7th International Graptolite Conference and Field Meeting of the International Subcommission on Silurian Stratigraphy. Serie Correlación geológica, **18**, 139–144.

Lehnert, O., Frýda, J., Buggisch, W., Munnecke, A., Nützel, A, Kříž, J. and Manda, S. 2007. $\delta^{13}C$ records across the late Silurian Lau event: new data from middle palaeo-latitudes of northern peri-Gondwana (Prague Basin, Czech Republic). *Palaeogeography, Palaeoclimatology, Palaeoecology*, **245**, 227–244, https://doi.org/10.1016/j.palaeo.2006.02.022

Lindskog, A., Young, S.A. *et al.* 2023. Oxygenation of the Baltoscandian shelf linked to Ordovician biodiversification. *Nature Geoscience*, **16**, 1047–1053, https://doi.org/10.1038/s41561-023-01287-z

Lohmann, K.C. 1988. Diagenetic systems and their application in studies of paleokarst. *In*: James, N.P. and Choquette, P.W. (eds) *Paleokarst*. Springer, 58–80, https://doi.org/10.1007/978-1-4612-3748-8_3

Lowery, C.M., Bralower, T.J. *et al.* 2023. Rapid recovery of life at ground zero of the end-Cretaceous mass extinction. *Nature*, **558**, 288–291, https://doi.org/10.1038/s41586-018-0163-6

Lu, W., Wörndle, S. *et al.* 2017. Iodine proxy evidence for increased ocean oxygenation during the Bitter Springs Anomaly. *Geochemical Perspective Letters*, **5**, 53–57, https://doi.org/10.7185/geochemlet.1746

Lu, W., Ridgwell, A. *et al.* 2018. Late inception of a resiliently oxygenated upper ocean. *Science*, **361**, 174–177, https://doi.org/10.1126/science.aar5372

Lu, Z., Jenkyns, H.C. and Rickaby, R.E.M. 2010. Iodine to calcium ratios in marine carbonate as a paleo-redox proxy during oceanic anoxic events. *Geology*, **38**, 1107–1110, https://doi.org/10.1130/G31145.1

Lu, Z., Hoogakker, B.A.A. *et al.* 2016. Oxygen depletion recorded in upper waters of the glacial Southern Ocean. *Nature Communications*, **7**, 1–8, https://doi.org/10.1038/ncomms11146

Manda, Š. 2008. Palaeoecology and palaeogeographic relations of the Silurian phragmoceratids (Nautiloidea, Cephalopoda) of the Prague Basin (Bohemia). *Bulletin of Geosciences*, **83**, 39–62, https://doi.org/10.3140/bull.geosci.2008.01.039

Manda, Š. and Frýda, J. 2014. Evolution of the late Ludlow to early Lochkovian brachiopod, trilobite and bivalve communities of the Prague Basin and their link with the global carbon cycle. *Geologiska Föreningens i Stockholm Förhandlingar*, **136**, 179–184, https://doi.org/10.1080/11035897.2014.882404

Manda, Š. and Kříž, J. 2006. Environmental and biotic changes in subtropical isolated carbonate platforms during the Late Silurian Kozlowskii Event, Prague Basin. *Geologiska Föreningens i Stockholm Förhandlingar*, **128**, 161–168, https://doi.org/10.1080/11035890601282161

Manda, Š., Štorch, P., Slavík, L., Frýda, J., Kříž, J. and Tasáryová, A. 2012. The graptolite, conodont and sedimentary record through the late Ludlow Kozlowskii Event (Silurian) in the shale-dominated succession of Bohemia. *Geological Magazine*, **149**, 507–531, https://doi.org/10.1017/S0016756811000847

März, C., Poulton, S.W., Beckman, B., Küster, K., Wagner, T. and Kasten, S. 2008. Redox sensitivity of P cycling during marine black shale formation: dynamics of sulfidic and anoxic, non-sulfidic bottom waters. *Geochimica et Cosmochimica Acta*, **72**, 3703–3717, https://doi.org/10.1016/j.gca.2008.04.025

McAdams, N.E.B., Cramer, B.D., Bancroft, A.M., Melchin, M.J., Devera, J.A. and Day, J.E. 2019. Integrated $\delta^{13}C_{carb}$, conodont, and graptolite biogeochemistry of the Silurian from the Illinois Basin and stratigraphic revision of the Bainbridge Group. *GSA Bulletin*, **113**, 335–352, https://doi.org/10.1130/B32033.1

McLennan, S.M. 2001. Relationships between the trace element composition of sedimentary rocks and upper continental crust. *Geochemistry, Geophysics, Geosystems*, **2**, 2000GC000109, https://doi.org/10.1029/2000GC000109

Mergl, M., Frýda, J. and Kubajko, M. 2018. Response of organophosphatic brachiopods to the mid-Ludfordian (late Silurian) carbon isotope excursion and associated extinction events in the Prague Basin (Czech Republic). *Bulletin of Geosciences*, **93**, 369–400, https://doi.org/10.3140/bull.geosci.1710

Meyer, K.M. and Kump, L.R. 2008. Oceanic euxinia in earth history: causes and consequences. *Annual Review of Earth and Planetary Sciences*, **36**, 251–288, https://doi.org/10.1146/annurev.earth.36.031207.124256

Morford, J.L. and Emerson, S. 1999. The geochemistry of redox sensitive trace metals in sediments. *Geochimica et Cosmochimica Acta*, **63**, 1735–1750, https://doi.org/10.1016/S0016-7037(99)00126-X

Munnecke, A., Samtleben, C. and Bickert, T. 2003. The Ireviken Event in the lower Silurian of Gotland, Sweden – relation to similar Palaeozoic and Proterozoic events. *Palaeogeography, Palaeoclimatology, Palaeoecology*, **195**, 99–124, https://doi.org/10.1016/S0031-0182(03)00304-3

Owens, J.D., Gill, B.C. *et al.* 2013. Sulfur isotopes track the global extent and dynamics of euxinia during Cretaceous oceanic anoxic event 2. *Proceedings of the National Academy of Sciences of the USA*, **110**, 18407–18412, https://doi.org/10.1073/pnas.1305304110

Owens, J.D., Reinhard, C.T., Rohrssen, M., Love, G.D. and Lyons, T.W. 2016. Empirical links between trace metal cycling and marine microbial ecology during a large perturbation to Earth's carbon cycle. *Earth and Planetary Science Letters*, **449**, 407–417, https://doi.org/10.1016/j.epsl.2016.05.046

Owens, J.D., Lyons, T.W., Hardisty, D.S., Lowery, C.M., Lu, Z., Lee, B. and Jenkyns, H.C. 2017. Patterns of local and global redox variability during the Cenomanian–Turonian boundary event (ocean anoxic event 2) recorded in carbonates and shales from central Italy. *Sedimentology*, **64**, 168–185, https://doi.org/10.1111/sed.12352

Pasquier, V., Bryant, R.N., Fike, D.A. and Halevy, I. 2021. Strong local, not global, controls on marine pyrite sulfur isotopes. *Science Advances*, **7**, eabb7403, https://doi.org/10.1126/sciadv.abb7403

Poulton, S.W. and Canfield, D.E. 2005. Development of a sequential extraction procedure for iron: implications for iron partitioning in continentally derived particulates. *Chemical Geology*, **214**, 209–221, https://doi.org/10.1016/j.chemgeo.2004.09.003

Present, T.M., Paris, G., Burke, A., Fischer, W.W. and Adkins, J.F. 2015. Large carbonate associated sulfate isotopic variability between brachiopods, micrite, and other sedimentary components in Late Ordovician strata. *Earth and Planetary Science Letters*, **432**, 187–198, https://doi.org/10.1016/j.epsl.2015.10.005

Railsback, L.B., Holland, S.M., Hunter, D.M., Jordan, E.M., Diaz, J.R. and Crowe, D.E. 2003. Controls on geochemical expression of subaerial exposure in Ordovician limestones from the Nashville Dome, Tennessee, USA. *Journal of Sedimentary Research*, **73**, 790–805, https://doi.org/10.1306/020503730790

Raiswell, R. and Canfield, D.E. 1998. Sources of iron for pyrite formation in marine sediments. *American Journal of Science*, **298**, 219–245, https://doi.org/10.2475/ajs.298.3.219

Raiswell, R., Newton, R., Bottrell, S.H., Coburn, P.M., Briggs, D.E.G., Bond, D.P.G. and Poulton, S.W. 2008. Turbidite depositional influences on the diagenesis of Beecher's Trilobite Bed and the Hunsruck Slate: sites of soft tissue pyritization. *American Journal of Science*, **308**, 105–129, https://doi.org/10.2475/02.2008.01

Raiswell, R., Hardisty, D.S. *et al.* 2018. The iron paleoredox proxies: a guide to the pitfalls, problems and proper practice. *American Journal of Science*, **318**, 491–526, https://doi.org/10.2475/05.2018.03

Richardson, J.A., Newville, M., Lanzirotti, A., Webb, S.M., Rose, C.V., Catalano, J.G. and Fike, D.A. 2019. Depositional and diagenetic constraints on the abundance and spatial variability of carbonate-associated sulfate. *Chemical Geology*, **523**, 59–72, https://doi.org/10.1016/j.chemgeo.2019.05.036

Rölich, P. 2007. Structure of the Prague Basin: the deformation diversity and its causes (the Czech Republic). *Bulletin of Geosciences*, **82**, 175–182, https://doi.org/10.3140/bull.geosci.2007.02.175

Rose, C.V., Fischer, W.W., Finnegan, S. and Fike, D.A. 2019. Records of carbon and sulfur cycling during the Silurian Ireviken Event in Gotland, Sweden. *Geochimica et Cosmochimica Acta*, **246**, 299–316, https://doi.org/10.1016/j.gca.2018.11.030

Rudnick, R.L. and Gao, S. 2003. The composition of the continental crust. *In*: Holland, H.D. and Turekian, K.K. (eds) *Treatise on Geochemistry, Vol. 3, The Crust*. Elsevier-Pergamon, 1–64, https://doi.org/10.1016/b0-08-043751-6/03016-4

Saltzman, M.R. 2001. Silurian delta C-13 stratigraphy: a view from North America. *Geology*, **29**, 671–674, https://doi.org/10.1130/0091-7613(2001)029<0671:SCSAVF>2.0.CO;2

Saltzman, M.R. 2002. Carbon isotope ($\delta^{13}C$) stratigraphy across the Silurian–Devonian transition in North America: evidence for a perturbation of the global carbon cycle. *Palaeogeography, Palaeoclimatology, Palaeoecology*, **187**, 83–100, https://doi.org/10.1016/S0031-0182(02)00510-2

Saltzman, M.R. and Thomas, E. 2012. Carbon isotope stratigraphy. *In*: Goldstein, F.M., Ogg, J.G. and Schmitz, M. (eds) *The Geologic Time Scale 2012*. Elsevier, 207–267, https://doi.org/10.1016/B978-0-444-59425-9.00011-1

Scotese, C.R. 2014. *Atlas of Silurian and Middle–Late Ordovician Paleogeographic Maps (Mollweide Projection), Maps 73–80. The Early Paleozoic, PALEOMAP Atlas for ArcGIS Vol. 5*. PALEOMAP Project, Evanston, IL, https://doi.org/10.13140/2.1.1087.2324

Sepkoski, J.J.,Jr 1996. Patterns of Phanerozoic extinction: a perspective from global databases. *In*: Walliser, O.H. (ed.) *Global Events and Event Stratigraphy in the Phanerozoic*. Springer, Berlin, 35–51, https://doi.org/10.1007/978-3-642-79634-0_4

Sim, M.S. 2019. Effect of sulfate limitation on sulfur isotope fractionation in batch cultures of sulfate reducing bacteria. *Geosciences Journal*, **23**, 687–694, https://doi.org/10.1007/s12303-019-0015-x

Sim, M.S., Ono, S. and Hurtgen, M.T. 2015. Sulfur isotope evidence for low and fluctuating sulfate levels in the Late Devonian ocean and the potential link with the mass extinction event. *Earth and Planetary Science Letters*, **419**, 52–62, https://doi.org/10.1016/j.epsl.2015.03.009

Slavík, L, Štorch, P., Manda, Š. and Frýda, J. 2014. Integrated stratigraphy of the Ludfordian in the Prague Synform. *Geologiska Föreningens i Stockholm Förhandlingar*, **136**, 238–242, https://doi.org/10.1080/11035897.2013.851733

Sperling, E.A., Melchin, M.J. *et al.* 2021. A long-term record of early to mid-Paleozoic marine redox change. *Science Advances*, **7**, eabf4382, https://doi.org/10.1126/sciadv.abf4382

Sproson, A.D., Pogge von Strandmann, P.A.E. *et al.* 2022. Osmium and lithium isotope evidence for weathering feedbacks linked to orbitally paced organic carbon burial and Silurian glaciations. *Earth and Planetary Science Letters*, **577**, 117260, https://doi.org/10.1016/j.epsl.2021.117260

Stampfli, G.M., Raumer, J.F. and Borel, G.D. 2002. Paleozoic evolution of pre-Variscan terranes: from Gondwana to the Variscan collision. *Geological Society of America, Special Papers*, **364**, 263–280, https://doi.org/10.1130/0-8137-2364-7.263

Štorch, P. 1995. Upper Silurian (upper Ludlow) graptolites of the *N. inexpectatus* and *N. kozlowskii* biozones from Kosov Quarry near Beroun (Barrandian area, Bohemia). *Bulletin of Geosciences, Czech Geological Survey*, **70**, 65–89.

Štorch, P. 1998. VIII. Volcanism. *In*: Chlupáč, I., Havlíček, V., Kříž, J., Kukal, Z. and Štorch, P. (eds) *Paleozoic of the Barrandian (Cambrian to Devonian)*. Czech Geological Survey, 149–164.

Stricanne, L., Munnecke, A. and Pross, J. 2006. Assessing mechanisms of environmental change: palynological signals across the Late Ludlow (Silurian) positive isotope excursion ($\delta^{13}C$, $\delta^{18}O$) on Gotland, Sweden. *Palaeogeography, Palaeoclimatology, Palaeoecology*, **230**, 1–31, https://doi.org/10.1016/j.palaeo.2005.07.003

Suchy, V., Sykorová, I., Stejskal, M., Šafanda, J., Machovič, V. and Novotná, M. 2002. Dispersed organic matter from Silurian shales of the Barrandian Basin, Czech Republic: optical properties, chemical composition, and thermal maturity. *International Journal of Coal Geology*, **53**, 1–25, https://doi.org/10.1016/S0166-5162(02)00137-4

Swart, P.K. and Eberli, G. 2005. The nature of the $\delta^{13}C$ of periplatform sediments: implications for stratigraphy and the global carbon cycle. *Sedimentary Geology*, **175**, 115–129, https://doi.org/10.1016/j.sedgeo.2004.12.029

Talent, J.A., Mawson, R., Andrew, A.S., Hamilton, P.J. and Whitford, D.J. 1993. Middle Paleozoic extinction events: faunal and isotopic data. *Palaeogeography, Palaeoclimatology, Palaeoecology*, **104**, 139–152, https://doi.org/10.1016/0031-0182(93)90126-4

Tasáryová, Z., Schnabl, P. *et al.* 2014. Gorstian palaeoposition and geotectonic setting of Suchomasty Volcanic Centre (Silurian, Prague Basin, Teplà-Barrandian Unit, Bohemian Massif). *Geologiska Föreningens i Stockholm Förhandlingar*, **136**, 262–265, https://doi.org/10.1080/11035897.2013.879735

Tasáryová, Z., Janoušek, V. and Frýda, J. 2018. Failed Silurian continental rifting at the NW margin of Gondwana: evidence from basaltic volcanism of the Prague Basin (Teplá-Barrandian Unit, Bohemian Massif). *International Journal of Earth Sciences*, **107**, 1231–1266, https://doi.org/10.1007/s00531-017-1530-5

Taylor, S.R. and McLennan, S.M. 1995. The geochemical the continental evolution crust. *Reviews in Mineralogy and Geochemistry*, **33**, 241–265.

Tonarová, P., Eriksson, M.E. and Hints, O. 2012. A jawed polychaete fauna from the late Ludlow Kozlowskii event interval in the Prague Basin (Czech Republic). *Bulletin of Geosciences, Czech Geological Survey*, **87**, 713–732, https://doi.org/10.3140/bull.geosci.1317

Tribovillard, N., Algeo, T.J., Lyons, T.W. and Ribolleau, A. 2006. Trace metals as paleoredox and paleoproductivity proxies: an update. *Chemical Geology*, **232**, 12–32, https://doi.org/10.1016/j.chemgeo.2006.02.012

Urbanek, A. 1993. Biotic crises in the history of the upper Silurian graptoloids: a paleobiological model. *Historical Biology*, **7**, 29–50, https://doi.org/10.1080/10292389309380442

Vacek, F. and Žák, J. 2019. A lifetime of the Variscan orogenic plateau from uplift to collapse as recorded by the Prague Basin, Bohemian Massif. *Geological Magazine*, **156**, 485–509, https://doi.org/10.1017/S0016756817000875

Wotte, T., Shields-Zhou, G.A. and Strauss, H. 2012. Carbonate-associated sulfate: experimental comparisons of common extraction methods and recommendations toward a standard analytical protocol. *Chemical Geology*, **326–327**, 132–144, https://doi.org/10.1016/j.chemgeo.2012.07.020

Young, S.A., Kleinberg, A. and Owens, J.D. 2019. Geochemical evidence for expansion of marine euxinia during an early Silurian (Llandovery–Wenlock boundary) mass extinction. *Earth and Planetary Science Letters*, **513**, 187–196, https://doi.org/10.1016/j.epsl.2019.02.023

Zhang, F., Frýda, J. *et al.* 2022. Marine anoxia as a trigger for the largest Phanerozoic positive carbon isotope excursion: evidence from carbonate barium isotope records. *Earth and Planetary Science Letters*, **584**, 117421, https://doi.org/10.1016/j.epsl.2022.117421